



Research article

Non-isocyanate polyurethane-co-polyglycolic acid electrospun nanofiber membrane wound dressing with high biocompatibility, hemostasis, and prevention of chronic wound formation

Fan Ge^a, Tong Wan^{a,b,*}, Linling Kong^a, Bowen Xu^a, Mengxue Sun^a, Biao Wang^a, Shubo Liang^a, Hao Wang^c, Xia Zhao^c

^a College of Chemical Engineering and Material Science, Tianjin University of Science and Technology TEDA, No. 29, 13th Street, Teda Street, Binhai New District, Tianjin, 300457, PR China

^b State Key Laboratory of Biobased Fiber Manufacturing Technology, Tianjin, 300457, PR China

^c College of Food Science and Engineering, Tianjin University of Science and Technology TEDA, No. 29, 13th Street, Teda Street, Binhai New District, Tianjin, 300457, PR China

ARTICLE INFO

Keywords:

Wound management
Nanofiber
Non-isocyanate polyurethane
Polyglycolic acid
Curcumin
Biomarker

ABSTRACT

The prevention of chronic wound formation has already been a primary subject in wound management, particularly for deep wounds. The electrospun nanofiber membranes hold tremendous potential in the prevention of chronic wounds due to their micro/nano pore structures. Currently, many natural and synthetic materials have been utilized in the fabrication of nanofiber membranes. However, striking a balance between the structural stability and the biocompatibility remains challenging. It is necessary not only to ensure the long-term durability of nanofiber membranes but also to enhance their biocompatibility for alleviating patients' suffering. In this study, we reported a nanofiber membrane dressing with excellent biocompatibility and mechanical properties, which is potential for the treatment of deep wounds. The basal material chosen for the preparation of the nanofiber membrane was a co-polyester (NI-LPGD5) synthesized by non-isocyanate polyurethane (NIPU) and polyglycolic acid with a dihydroxy structure (LPGD—synthesized from glycolic acid and neopentyl glycol). Moreover, curcumin was also added as a bioactive substance to enhance the pro-healing effect of dressings. The physicochemical properties of the prepared nanofiber membranes were characterized through various physicochemical tools. Our results demonstrated that the NI-LPGD5 co-polymer can be electrospun into smooth fibers. Meanwhile, curcumin-loaded nanofiber membranes (Cur/NI-LPGD5) also exhibited a favorable microscopic morphology. The fabricated membranes exhibited suitable mechanical properties, outstanding hygroscopic-swelling rate and water vapor transmittance. Besides, *in vitro* cell culturing, the cells on the NI-LPGD5 membrane maintained their maximum viability. The potential of *in vivo* wound healing was further demonstrated through animal experiments. The experimental results showed that the nanofiber membranes effectively prevented chronic wounds from forming and promoted granulation tissue growth without replacing the dressing throughout the healing process. We also found that these nanofiber membranes could effectively promote the expression of related biomarkers to accelerate wound healing, particularly the Cur/NI-LPGD5 membrane. In conclusion, the fabricated membranes possess suitable physicochemical properties and promising bioactivity. As a result, it effectively prevented the

* Corresponding author.

E-mail address: wantong@tust.edu.cn (T. Wan).

formation of chronic wounds and demonstrated significant potential in reducing the frequency of dressing changes.

1. Introduction

The skin is the largest organ of the human body, accounting for 15 % of its total body mass, serving as the first line of defense against external damage and bacterial invasion [1,2]. The skin also plays a crucial role in body temperature regulation, sensation, immunity, and fluid balance [1]. Damage to the skin can lead to adverse health effects, particularly if wounds become chronic. In such cases, exogenous bacterial infection due to poor hemostasis or frequent dressing replacement would significantly increase the risk of chronic wound formation [2–6]. Therefore, there is an urgent need in modern medicine to design wound dressings that stop bleeding quickly, resist bacterial invasion, and reduce the need for replacement. Currently, wound dressings such as gauze, synthetic fiber cloth, foam, and hydrogel are widely used in wound healing [6–10]. However, these dressings cannot simultaneously meet the above-mentioned requirements of rapidly absorbing wound exudate, preventing exogenous bacteria from invading, and minimizing dressing replacement during use [1,11,12]. Electrospun nanofiber membranes may potentially meet these requirements, as their high specific surface area can absorb a large amount of wound exudates (e.g., platelets), promptly stopping bleeding, and promoting cell migration and proliferation [13]. Furthermore, their micro/nano pores can prevent invasion by exogenous microorganisms, reducing the frequency of dressing replacement. These pores have a structure similar to that of the extracellular matrix (ECM), which can effectively promote wound healing [6,14,15]. These characteristics make electrospun nanofiber membranes an ideal candidate for wound dressing.

Currently, various natural and synthetic materials, such as chitosan, collagen, polycaprolactone, polyvinyl alcohol, and polylactic acid, have been utilized in developing nanofiber membrane wound dressings [16–20]. However, the electrospun nanofiber membranes composed of natural polymers generally exhibit suboptimal mechanical properties. Meanwhile, the rapid degradation rate of natural materials also leads to their limited durability. Polyurethane (PU), as a synthetic material, has been widely used in the medical field, as it has excellent mechanical flexibility, hydrophilicity, and physical and chemical properties, and its synthetic raw materials can be selected according to requirements [21,22]. However, PU production requires toxic diisocyanate compounds, which can cause irreversible damage to the environment and human health [23–25]. Non-isocyanate polyurethane (NIPU) may be used as a significant material for wound dressings in the future. Nevertheless, synthetic materials generally lack natural cell recognition receptors, which will generally cause immune rejection upon contact with the body.

Studies have shown that hydrophilic and biocompatible materials are conducive to contact with cells directly, alleviate inflammatory reactions, and promote cell proliferation and migration [26–28], which is crucial for wound dressings to effectively promote wound healing [22,29]. At the same time, excellent biocompatibility also helps to reduce the frequency of dressing replacement. Therefore, at the early stages of wound dressing design, hydrophilic and biocompatible substances should be considered for use as basal materials. Polyglycolic acid (PGA) is widely used in surgery and regenerative medicine due to its hydrophilicity and biocompatibility [28–33]. PGA is a safe metabolic molecule that can come into direct contact with cells, reducing immune rejection in the body [30]. Current applied researches on PGA focus on using high-molecular-weight PGA, which has poor toughness, high cost, and poor processability; it is also susceptible to damage during heating, making it difficult to be processed into nanofibrous materials [31–33]. Therefore, we have synthesized a low-molecular-weight PGA diol (LPGD) that is more affordable than conventional PGA. Additionally, the structure of LPGD allows it to be easily copolymerized with other diols, making it a more versatile material. However, integrating LPGD with NIPU remains a challenging task.

In this study, we used glycolic acid (GA) and neopentyl glycol (NPG) to prepare LPGD. Next, we synthesized NIPU using ethylene carbonate (EC), 1,6-hexanediamine (1,6-HDA), and polyethylene glycol 1000 (PEG1000). We then dissolved LPGD and NIPU in hexafluoroisopropanol (HFIP) solvent and used sebacyl chloride (SAC) as a chain extender to obtain non-isocyanate polyurethane-co-polyglycolic acid (NI-LPGD) through an amidation reaction. Finally, an electrospinning machine was used to prepare NIPU and NI-LPGD nanofiber membranes with HFIP as the solvent. Afterwards, curcumin was added to prepare the Cur/NI-LPGD nanofiber membrane. A variety of instruments and techniques were used to systematically analyze the morphology, chemical structure, and mechanical and thermal properties of LPGD, NIPU, and NI-LPGD, as well as the microstructure, hygroscopic-swelling rate, and water vapor transmittance of the nanofibrous films. The safety and efficacy of the nanofiber membrane were confirmed by analyzing hemostasis, wound contraction, histomorphology, and biomarkers in hemorrhaging liver mouse and full-thickness skin defect models.

2. Materials and methods

2.1. Materials

GA was provided by Morinaga Milk Co., Ltd., and pre-dried in an oven before use. NPG and TEA were provided by Macklin Biochemical Technology Co., Ltd., Shanghai. PEG1000, HFIP, deuterated dimethyl sulfoxide (DMSO- d_6), and SAC were provided by Merger Technologies Co., Ltd., Shanghai. 1,6-HDA and EC were provided by Bidepharm Co., Ltd. Zinc acetate dihydrate ($(\text{CH}_3\text{COO})_2\text{Zn}\cdot 2\text{H}_2\text{O}$), serving as a catalyst for esterification and transesterification reactions, was provided by Tianjin Sitong Chemical Plant, Bei Chen District, Tianjin. Stannous chloride dihydrate ($\text{SnCl}_2\cdot 2\text{H}_2\text{O}$) was provided by Tianjin North Tianyi Chemical. Toluene was provided by Tianjin Damao Chemical. Curcumin was provided by Shanghai Xu Shuo Biotechnology Co., Ltd. Phosphate

buffer solution (PBS, pH = 7.4) was provided by Sheng Shi Standard (Xiamen) Technology Co., Ltd.

2.2. Synthesis of low-molecular-weight polyglycolic acid diol (LPGD)

GA and NPG were used as raw materials for LPGD synthesis, with $(\text{CH}_3\text{COO})_2\text{Zn}\cdot 2\text{H}_2\text{O}$ serving as the catalyst. The entire reaction process was divided into two parts: the normal pressure reaction part and the low-pressure reaction part. During the normal pressure reaction, the temperature ranged from 120 °C to 150 °C. During the low-pressure reaction, the temperature ranged from 150 °C to 190 °C, while maintaining a reaction pressure of 600 pa. Additional details are available in the Materials and Methods section of the Supporting Information (SI).

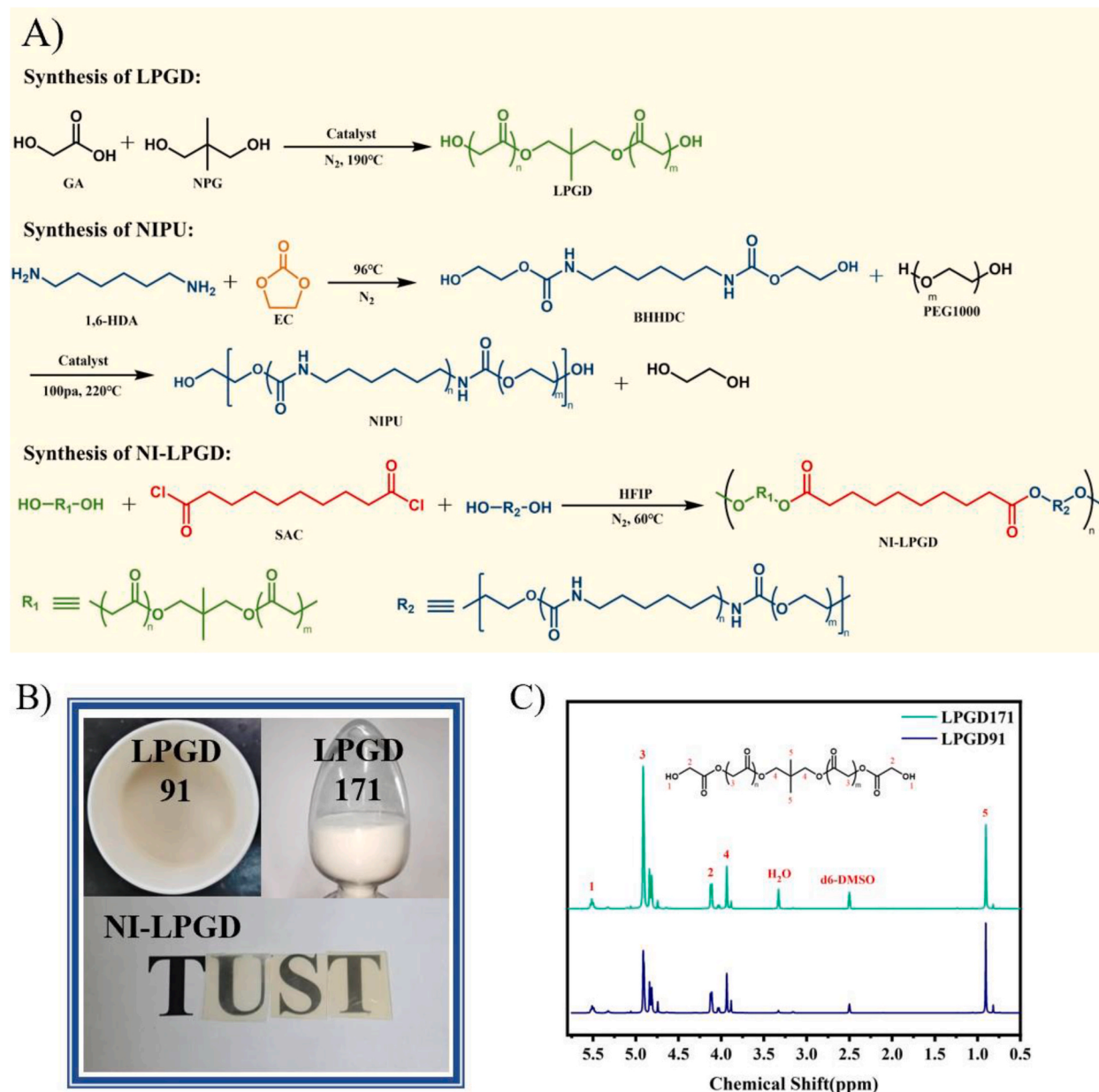


Fig. 1. Synthesis equations and presentation of work: A) Synthesis equations of LPGD, NIPU, and NI-LPGD; B) Sample display: LPGD91 viscous liquid, LPGD171 solid powder, and NI-LPGD transparent film; C) ^1H NMR spectra of LPGD91 and LPGD171.

2.3. Synthesis of bis (2-hydroxyethyl) hexane-1,6-diylidicarbamate (BHHDC)

The synthesis of BHHDC is described in Ref. [34]. EC and 1,6-HAD were used as raw materials for BHHDC synthesis. After heating the reaction to 80 °C for 2 h, it was further heated to 96 °C for 2 h. After that, the reaction was continued for 30 min at 80 °C by adding 180 g of deionized water and subsequently cooled to room temperature. The mixture was then stored in a refrigerator and recrystallized the next day. Additional details are available in the Materials and Methods section of the SI.

2.4. Synthesis of non-isocyanate polyurethane (NIPU)

The synthesis of NIPU is described in Ref. [34]. BHHDC and PEG1000 were used as raw materials for NIPU synthesis, with $\text{SnCl}_2 \cdot 2\text{H}_2\text{O}$ serving as the catalyst. The reaction temperature was 220 °C and the reaction pressure was 600 Pa. Additional details are available in the Materials and Methods section of the SI.

2.5. Synthesis of non-isocyanate polyurethane-co-polyglycolic acid (NI-LPGD)

LPGD171 and NIPU were used as raw materials for NI-LPGD synthesis, with HFIP serving as the solvent. The reaction was conducted at a temperature of 60 °C for 30 min. Among the NI-LPGD, the mass fraction of LPGD171 was from 5 wt% to 20 wt%, and they were named NI-LPGD5, NI-LPGD10, NI-LPGD15 and NI-LPGD20. Additional details are available in the Materials and Methods section of the SI.

2.6. Preparation of electrospun nanofiber membranes

The spinning solution was obtained by dissolving 0.5 g of NIPU or NI-LPGD5 in 4.5 g of HFIP. After the solute was completely dissolved, it was drawn into a 10-mL syringe. The voltage and propulsion speed for spinning were set at 17 kV and 0.4 mm/h, respectively. The film was spun onto release paper at a distance of 15 cm. Thus, NIPU and NI-LPGD5 nanofibrous membranes were prepared, respectively.

Cur/NI-LPGD5 nanofibrous membranes were prepared using the same method by dissolving 0.5 g of NI-LPGD5 and 0.025 g of curcumin in 4.5 g of HFIP.

2.7. In vitro physicochemical characteristics

The physicochemical characteristics of LPGD, NIPU, and NI-LPGD were analyzed by Fourier-transform infrared spectroscopy (FT-IR), ^1H nuclear magnetic resonance spectroscopy (^1H NMR), X-ray photoelectron spectroscopy (XPS), differential scanning calorimetry (DSC), thermogravimetry (TG), a universal tensile testing machine, and a contact angle-measuring instrument.

2.8. LPGD molecular weight

The average molecular weight of LPGD was calculated by ^1H NMR [35]. The samples were dissolved in $\text{DMSO}-d_6$, respectively. The hydrogen spectra of LPGD91 and LPGD171 were obtained using a ^1H NMR, as shown in Fig. 1C, with unique hydrogens marked. In this study, the number of repeat units of LPGD was calculated according to Equation (1) using the integrated area of the hydrogen atom on the methylene group at position 3 and the hydrogen atom on the methyl group at position 5. The average molecular weight of LPGD was calculated according to Equation (2):

$$\frac{X}{Y} = \frac{2n}{6} \rightarrow n = \frac{3X}{Y} \quad (1)$$

$$\overline{M}_n = 56n + 104 \quad (2)$$

where X represents the peak area of the methylene hydrogen atom, Y represents the peak area of the methyl hydrogen atom, and n represents the number of LPGD repeat units.

2.9. Diameter of nanofibers and porosity of nanofiber membranes

Using the ImageJ software, 150 fiber diameters were randomly selected from scanning electron microscopy (SEM) images of the NIPU, NI-LPGD5, and Cur/NI-LPGD5 nanofibrous membranes. The average fiber diameter, diameter distribution, and porosity of the nanofiber membranes were calculated using ImageJ software.

2.10. Mechanical properties of nanofiber membranes

The nanofiber films were sliced into 1 cm × 5 cm samples, with five samples prepared for each film. The tensile properties of the samples were tested on the universal tensile testing machine (CMT-4254) under a tensile speed of 5 mm/min and an effective clamping

distance of 4 cm.

2.11. Hygroscopic-swelling rate of nanofiber membranes

The hygroscopic-swelling rate experiments were conducted following Reference [36]. Weighed samples were added to flasks containing 20 mL of PBS (pH = 7.4), which were placed in a shaker for 24 h at 37 °C. The samples were then clamped with tweezers and suspended for 30 s. The samples were weighed after no liquid had dripped. Then the samples' hygroscopic-swelling rate was calculated according to Equation (3):

$$\text{weight}(\%) = \frac{w_{\text{wet}} - w_{\text{dry}}}{w_{\text{dry}}} \times 100\% \quad (3)$$

where w_{wet} is the wet weight of the sample after soaking in PBS solution for 24 h, and w_{dry} is the dry weight of the sample before soaking.

2.12. Water vapor transmittance (WVTR) of nanofiber membranes

The WVTR of NIPU, NI-LPGD5, and Cur/NI-LPGD5 nanofibrous membranes were measured using a Water Vapor Transmittometer (PERME W3/030) at a temperature of 38 °C and a relative humidity of 90 %.

2.13. Antibacterial activity evaluation of nanofiber membranes

The antibacterial method used in this study was the dilution coated plate method. *Escherichia coli* (ATCC 8739) and *Staphylococcus aureus* (ATCC 29213) were used to determine the antibacterial properties of NIPU, NI-LPGD5, and Cur/NI-LPGD5 nanofiber membranes [37]. Additional experimental details can be found in the Materials and Methods section of the SI. The bacterial killing rate of each nanofiber membrane was calculated according to Equation (4):

$$\text{Kill}(\%) = \frac{n_c - n_e}{n_c} \times 100\% \quad (4)$$

where n_c is the colony number of the control group, and n_e is the colony number of the experimental group.

2.14. Biocompatibility and cytotoxicity evaluation of nanofiber membranes

The biocompatibility and cytotoxicity of the NIPU and NI-LPGD5 nanofibrous membranes were assessed by directly contacting mouse fibroblasts (L929). The number of cells was also counted using ImageJ software. Additional experimental details can be found in the Materials and Methods section in the SI.

2.15. Evaluation of the hemostatic ability of nanofiber membranes

The *in vivo* hemostatic ability of the nanofiber membranes was evaluated according to Ref. [38]. Additional experimental details can be found in the Materials and Methods section of the SI.

2.16. Wound healing evaluation in a full-thickness skin defect model

Based on the literature [8], a full-thickness skin defect model was established using female KM mice weighing 30–40 g for wound-healing experiments. All animal experiments were approved by the Animal Ethics Committee of Chengdu Sunway Experimental Animal Co., Ltd. Additional details can be found in the Materials and Methods section of the SI.

2.17. Morphological evaluation of regenerated tissue

The samples collected on days 5, 10, and 15 were fixed with 4 % paraformaldehyde for 1 h. Before H&E staining, the samples were embedded in paraffin and then transected into 4 μm thick tissue sections. After that, the prepared tissue sections were dewaxed, rehydrated and stained with H&E. The nuclei were stained blue with hematoxylin, and the cytoplasm was stained red with eosin. All sections were analyzed and photographed using a microscope (IX53, Olympus, Japan).

2.18. Expression of biomarker involved in wound healing

The biomarker content of transforming growth factor-β1 (TGF-β1) and vascular endothelial growth factor (VEGF-A), which are two major growth factors in wound healing, was measured in the regenerated skin tissues collected. At the end of the full-thickness skin defect model experiments, the levels of TGF-β1 and VEGF-A in mice tissue samples were determined by enzyme-linked immunosorbent assay (ELISA) kits (Elabscience Biotechnology, Wuhan, China). The measurement was strictly carried out according to the

requirements of the kit manufacturer.

2.19. Statistical analysis

The data of this study were expressed as means \pm standard deviations (SDs). Statistical significance was calculated by one-way ANOVA using Origin (2021 version, USA) software. A value of $p < 0.05$ indicates a statistically significant difference.

3. Results and analysis

3.1. Synthesis of LPGD

In this study, a series of nanofiber membrane dressings with good flexibility, excellent biocompatibility, and toxicological safety was designed using LPGD and NIPU as base materials. The LPGD reaction scheme is shown in Fig. 1A. In this reaction, NPG was selected to react with GA to synthesize LPGD. The main reason for choosing NPG is its high boiling point, which allows it to be retained in the reaction system, as well as its low cost. Each LPGD sample was named according to the difference in the molar ratio of GA to NPG added. For example, as shown in Table 1, LPGD91 represents $n(\text{GA}):n(\text{NPG}) = 9:1$, and LPGD171 represents $n(\text{GA}):n(\text{NPG}) = 17:1$, which each shows different physical morphology. As shown in Fig. 1B, LPGD91 is a viscous liquid, and LPGD171 is a solid.

^1H NMR was used to verify the molecular weight of the synthesized LPGD. The ^1H NMR spectra of LPGD91 and LPGD171 are shown in Fig. 1C. $\text{DMSO-}d_6$ was used for the ^1H NMR test as a solvent, whose chemical shift was $\delta = 2.50$ ppm. The chemical shift at $\delta = 3.33$ ppm was attributed to water in the solvent. Five chemically equivalent hydrogen atoms were present in the structure of LPGD, which were mainly reflected in the ^1H NMR spectra at $\delta = 5.52$ ppm (H_1 , triple peak), $\delta = 4.12$ ppm (H_2 , double peak), $\delta = 4.91$ ppm (H_3 , single peak), $\delta = 3.94$ ppm (H_4 , single peak), and $\delta = 0.90$ ppm (H_5 , single peak). Thus, the positions of the H_1 to H_5 representing hydrogen in the NMR spectrum were identified, indicating that LPGD synthesis was successful. At the same time, in the ^1H NMR hydrogen spectrum, the peak area can roughly reflect the number of hydrogen atoms [35]; this feature can be used to estimate the molecular weight of the substance. In this study, we chose the hydrogen atom on the methylene group in the LPGD repeat unit and the hydrogen atom on the methyl group in the neopentyl glycol to calculate the molecular weight. Their integral areas are shown as Integrals 3 and 5 in Table 1, respectively. The average molecular weight of the LPGD obtained was calculated according to Equations (1) and (2).

3.2. Synthesis and characterization of NI-LPGD

LPGD cannot be electrospun due to its low toughness and low molecular weight. However, it can be copolymerized with NIPU to synthesize NI-LPGD to meet the spinning requirements. To explore the physicochemical properties of NI-LPGD, four kinds of NI-LPGD copolyesters with different LPGD mass fractions were designed in this study. As seen in Table 2, the LPGD mass fractions ranged from 5 wt% to 20 wt%. To synthesize these copolyesters, NIPU was first synthesized. The process began with the cyclic opening of EC and 1,6-HDA to produce BHHDC. Then, NIPU was obtained by a transesterification reaction with PEG1000. Then, SAC was used to link LPGD and NIPU to make NI-LPGD (Fig. 1A). TEA was added to the system as an acid binder to neutralize HCl produced by the amidation reaction and facilitate the reaction. The amount of SAC and TEA added was equal to that of LPGD. FT-IR, ^1H NMR, XPS, DSC, and TG were used to characterize the physicochemical properties of NI-LPGD.

The chemical structures of NIPU and NI-LPGD were confirmed by FT-IR, as shown in Fig. 2A. The peak at 3319 cm^{-1} is attributed to the stretching vibration peak of the terminal hydroxyl group or N-H in the ammonia ester bond. The peak at 2800 cm^{-1} to 3000 cm^{-1} is the methylene absorption peak. The two distinct peaks at 1738 cm^{-1} and 1536 cm^{-1} are the stretching vibration peak of the C=O bond of the carbamate group in polyurethane and the characteristic absorption peak of the -N-H- bond, respectively. The peaks at 1100 cm^{-1} are the stretching vibration peaks of the -C-O- single bond in LPGD and the ether bond (-C-O-C-) in PEG. This FT-IR pattern reveals the presence of aminoester, ester, and ether bonds in the structure of the synthesized NI-LPGD sample, indicating the successful introduction of LPGD and PEG.

The successful synthesis of NIPU and NI-LPGD was confirmed by ^1H NMR, as shown in Fig. 2B. The characteristic peaks of the methylene group of the BHHDC moiety in NIPU (number 1 of Fig. 2B) and the methylene group of the SAC moiety (number 2 of Fig. 2B) are seen at $\delta = 1.08$ ppm [39]. As seen in Fig. 2B, the integrated area of NI-LPGD5 at $\delta = 1.08$ ppm is significantly larger than that of NIPU, indicating that SAC was well involved in the reaction. In NIPU synthesis, a tail-biting reaction occurred to produce a urea bond according to the reaction scheme shown in Fig. 2C. Upon reviewing the relevant literature, $\delta = 5.70$ ppm was determined to be the position of the urea bond in the ^1H NMR map [40]. It is difficult to observe this peak in Fig. 2B, suggesting minimal side reaction during NIPU synthesis.

Table 1
LPGD formulation, MRI integral area, and molecular weight.

Sample	Molar Ratio $n(\text{GA}):n(\text{NPG})$	m_{GA} (g)	m_{NPG} (g)	Catalyst (g)	Integral 3	Integral 5	\bar{M}_n (g/mol)
LPGD91	9:1	116.7	17.7	0.2	10.9	6	500
LPGD171	17:1	150.8	14.7	0.3	23.2	6	900

Table 2
NI-LPGD synthetic formulation.

Sample	m_{LPGD171} (wt%)	m_{NIPU} (g)	m_{LPGD171} (g)	m_{SAC} (g)	m_{TEA} (g)
NI-LPGD5	5	9.5	0.5	0.17	0.07
NI-LPGD10	10	9	1	0.33	0.13
NI-LPGD15	15	8.5	1.5	0.49	0.21
NI-LPGD20	20	8	2	0.65	0.27

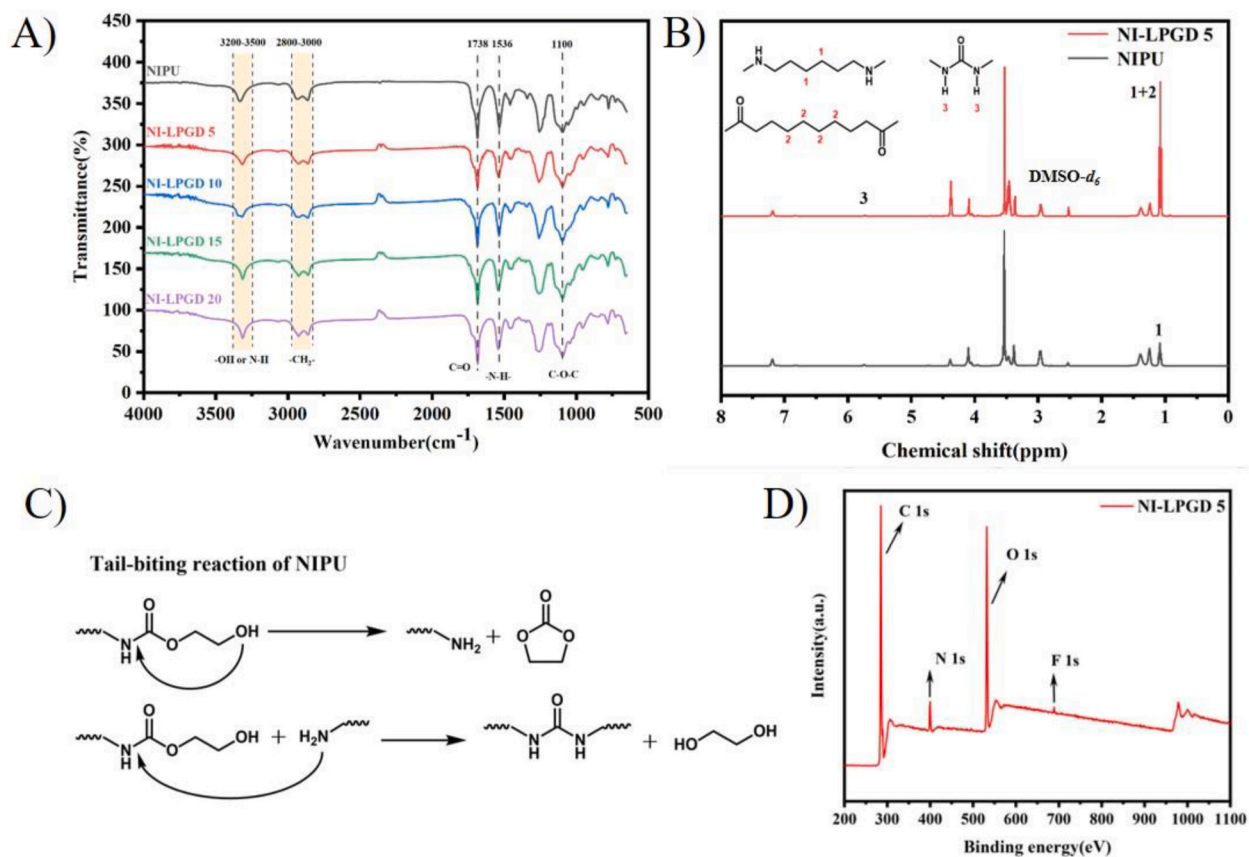


Fig. 2. Characterization of NI-LPGD: A) FT-IR spectra of NIPU and NI-LPGD; B) ¹H NMR curves of NIPU and NI-LPGD5; C) tail-biting reaction in NIPU synthesis; and D) NI-LPGD5 XPS curve.

XPS was used to perform an elemental analysis of NI-LPGD5, as shown in Fig. 2D. The main characteristic peaks are C 1s with a binding energy of 284.8 eV and O 1s with a binding energy of 532.1 eV. The typical peak of N 1s is relatively weak, whereas the characteristic peak intensity of F 1s is the lowest at 689 eV and can hardly be observed, indicating a low residual fluorine content in the synthesized NI-LPGD5.

We also tested the thermodynamic properties of NIPU and NI-LPGD. DSC and TG results are shown in Figs. S1 and S2 of the SI, respectively. The DSC curves show that these materials' glass transition temperature (T_g) is -40°C , indicating that the materials have good low-temperature flexibility. The melting point (T_m) of NIPU was determined to be 153°C . An increase in LPGD content caused the copolyester's T_m to first decrease before increasing, eventually displaying two melting points. This is because the introduction of LPGD, a solid polar substance, reduces the crystallinity of NIPU and decreases its melting point. With the increase of LPGD content, the crystalline region of LPGD in NI-LPGD increased, which showed that the copolyester had two melting points of 145°C and 152°C [41]. As can be seen from Fig. S2 of the SI, NIPU exhibited a 10% weight loss at a temperature of 255°C , whereas that of NI-LPGD exhibited a 10% weight loss at 272°C . This is because the thermal decomposition temperature of the ester bond in LPGD is higher than that of the carbamate bond in NIPU, which improves the heat resistance of NI-LPGD.

3.3. Physical properties of NIPU and NI-LPGD

As seen in Fig. 3A, NIPU and NI-LPGD5 demonstrated good mechanical properties. The tensile strength of NI-LPGD5 (11.8 ± 0.5

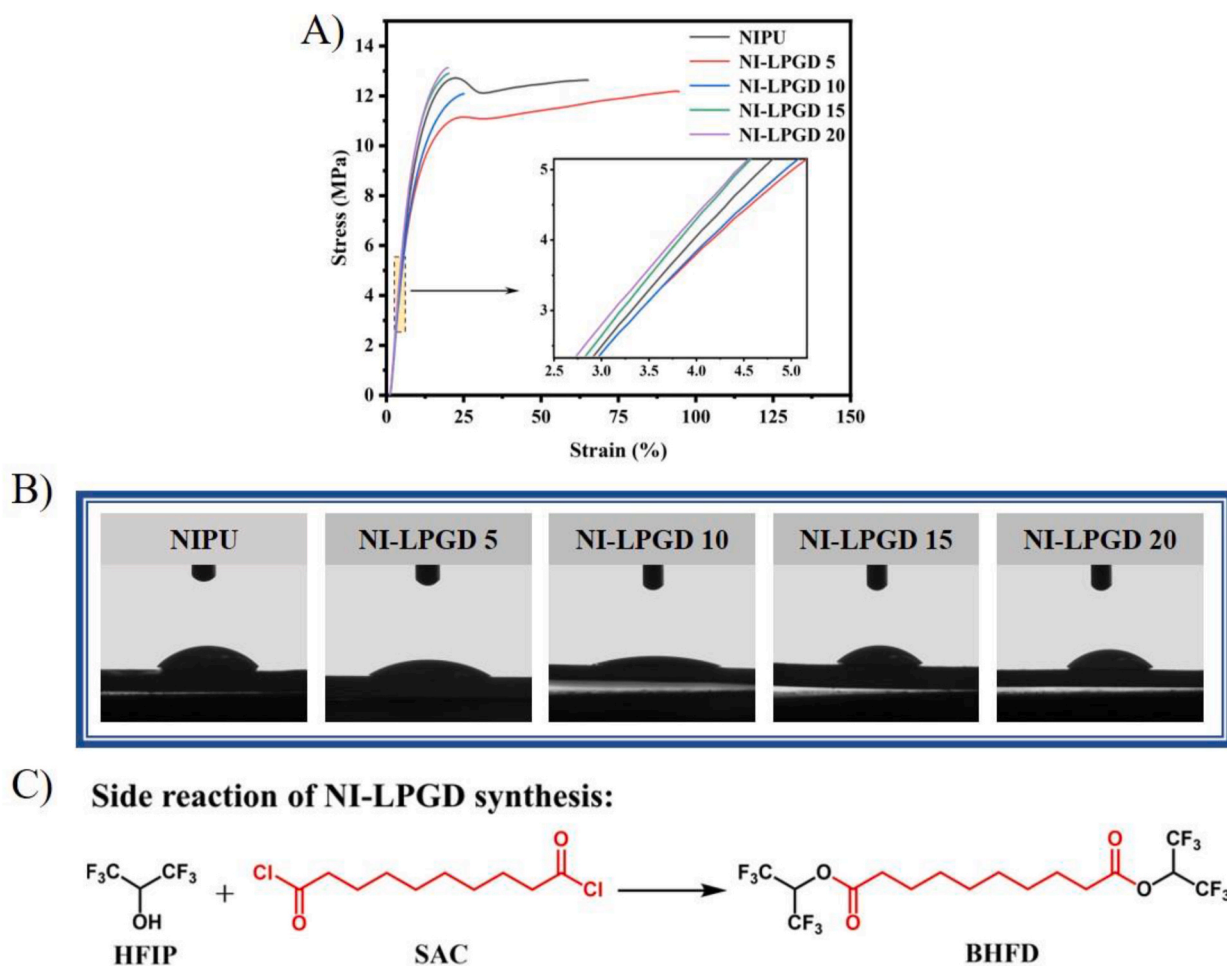


Fig. 3. Physical properties of NI-LPGD: A) Mechanical properties of NIPU and NI-LPGD; B) water contact angle map of NIPU and NI-LPGD; C) side reaction of NI-LPGD synthesis.

MPa) was lower than that of NIPU (12.1 ± 0.5 MPa), but the latter had the higher elongation at break (128.0 ± 23.7 %) than the former (81.9 ± 26.7 %). The tensile strength and elongation at break of the three groups of copolymers (NI-LPGD10 to NI-LPGD20) showed increasing and decreasing trends, respectively. The fracture mode of the materials changed from a ductile fracture of NI-LPGD5 to a

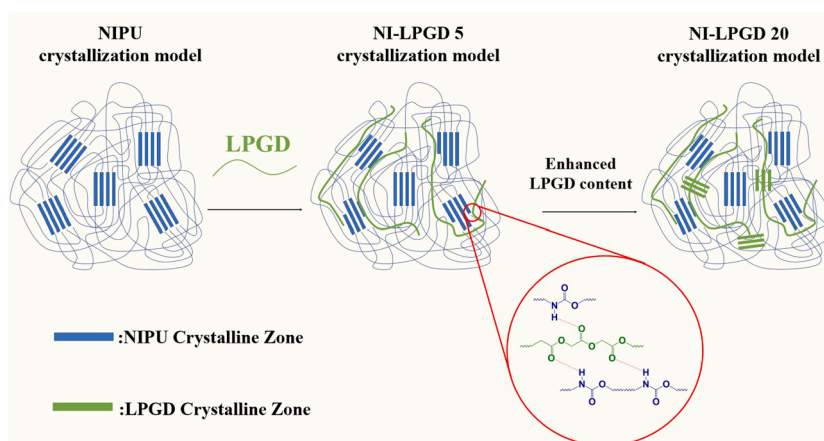


Fig. 4. Schematic diagram of crystallization of NIPU and NI-LPGD.

brittle fracture of NI-LPGD20. This is because, with the increase of LPGD content, the LPGD crystallization area in the copolyester becomes larger, thereby reducing the toughness of the copolyester. A schematic diagram of the crystallization of NIPU to NI-LPGD is shown in Fig. 4, the hydrogen bonding between the ester bond of LPGD and the carbamate bond of NIPU would result in a reduced crystallinity of NI-LPGD compared to that of NIPU. Simultaneously, due to the pronounced crystallization ability of LPGD, an increasing content of LPGD in NI-LPGD gradually leads to the formation of two crystal structures corresponding to NIPU and LPGD within NI-LPGD. The change in crystallinity between NIPU and NI-LPGD is shown in Fig. S3 of the SI, where the crystallization peak area from NIPU to NI-LPGD20 first decreases and then increases.

The hydrophilicity of NIPU and NI-LPGD was characterized in terms of water contact angle. As shown in Fig. 3B, NIPU and NI-LPGD

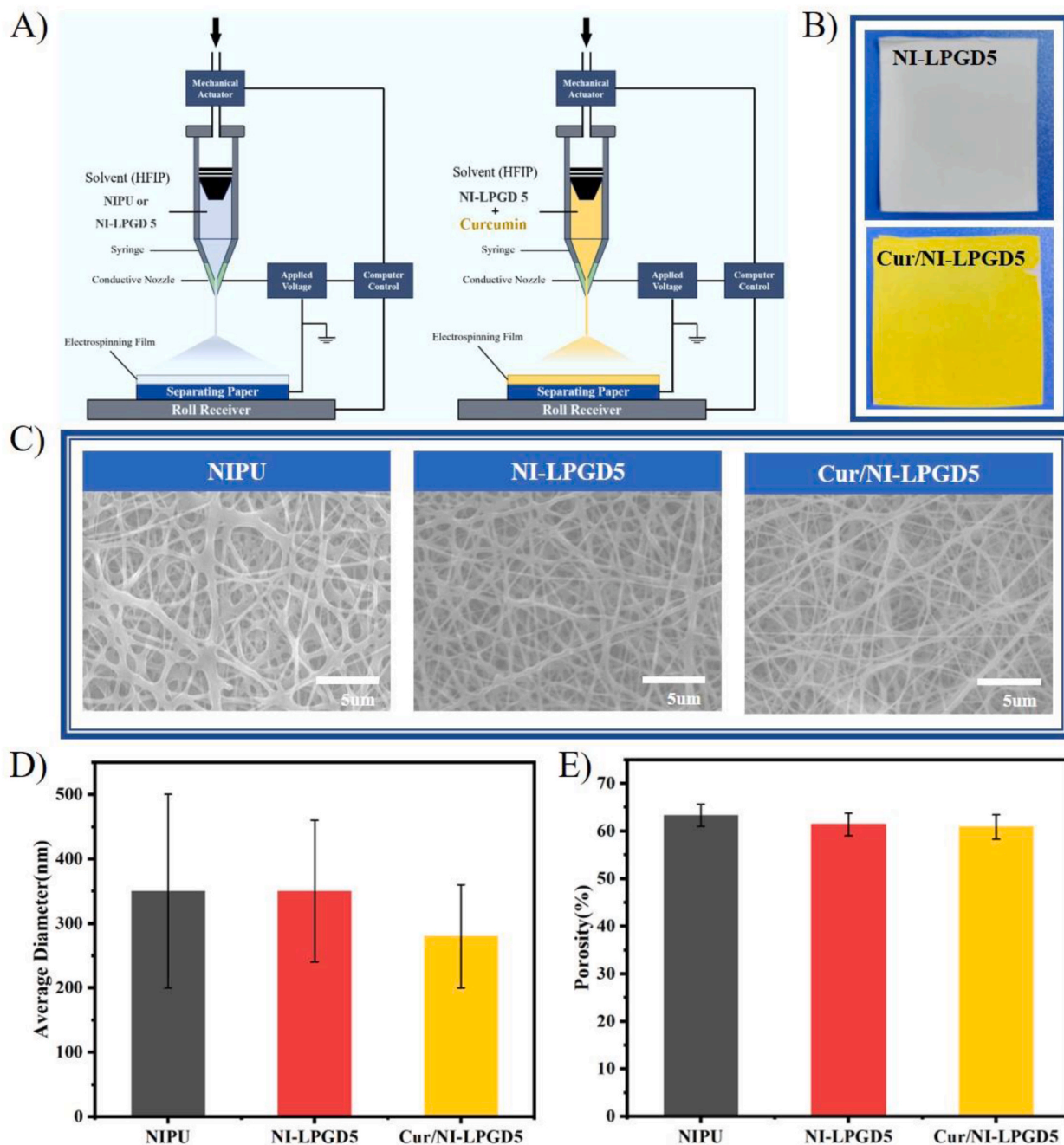


Fig. 5. Morphology and structure of nano electrospinning films: A) Schematic diagrams of NIPU, NI-LPGD5, and Cur/NI-LPGD5 electrospinning; B) NI-LPGD5 and Cur/NI-LPGD5 electrospun films; C) SEM and diameter distribution histogram of nanofiber membrane; D) mean diameter of nanofibers; and E) nanofiber membrane porosity.

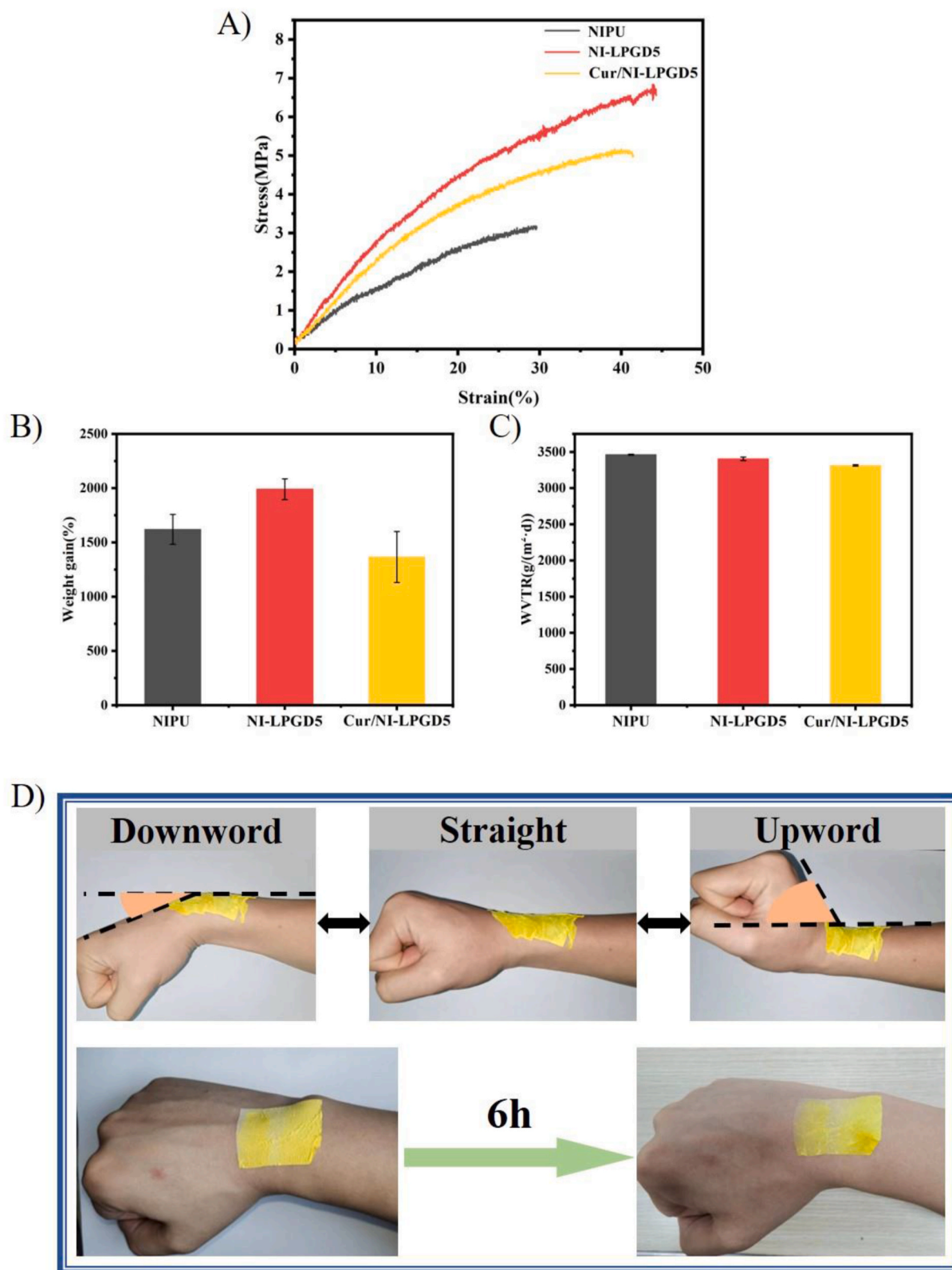


Fig. 6. Physical properties of the nanofiber membrane: A) stress-strain diagram of the nanofiber membrane; B) hygroscopic swelling rate of the nanofiber membrane; C) WVTR of the nanofiber film; D) adhesion effect of Cur/NI-LPGD5 nanofiber membrane on the human wrist.

all showed hydrophilic characteristics. The water contact angles of NI-LPGD5 (38°) and NI-LPGD10 (17°) were significantly smaller than that of NIPU (51°), indicating that the introduction of LPGD could well improve the hydrophilicity of the material. However, the water contact angles of NI-LPGD15 (40°) and NI-LPGD20 (44°) did not continue to decrease but increased. This is caused by the residual fluorine element in NI-LPGD, namely, the side reaction of the solvent (HFIP) with sebacyl chloride during the synthesis of NI-LPGD. Fig. 3C is the reaction equation diagram of side reaction of NI-LPGD synthesis.

3.4. Morphology and structure of nanofibrous membranes

The microstructures of the three prepared nanofiber membranes were observed. Fig. 5A shows a schematic diagram of the NIPU, NI-LPGD5, and Cur/NI-LPGD5 nanofiber films prepared by electrospinning. Fig. 5B shows the completed spun NI-LPGD5 nanofiber film and Cur/NI-LPGD5 nanofiber film. Fig. 5C shows the SEM and diameter distribution histograms of NIPU, NI-LPGD5, and Cur/NI-LPGD5 nanofibrous membranes. The surfaces of all the nanofiber samples were smooth and continuous, indicating that the electrospinning parameters were appropriate. The mean diameters of the NIPU, NI-LPGD5, and Cur/NI-LPGD5 nanofibers were 350 ± 150 nm, 350 ± 110 nm, and 280 ± 80 nm, as seen in Fig. 5D. We then calculated the porosity of the nanofiber membrane using ImageJ software, as shown in Fig. 5E. The porosities of these nanofiber membranes were all more than 60 %, which is consistent with values reported in the literature [42].

3.5. Physical properties of nanofiber membranes

The mechanical properties of the NIPU, NI-LPGD5, and Cur/NI-LPGD5 nanofiber membranes fabricated in this work are shown in Fig. 6A. The tensile strength of the NIPU nanofiber membrane was 3.4 ± 0.2 MPa, and its elongation at break was 34.2 ± 8.5 %. The tensile strength of the NI-LPGD5 nanofiber membrane was 6.5 ± 0.8 MPa, its elongation at break was 36.1 ± 5.5 %. The tensile strength of the Cur/NI-LPGD5 nanofiber membrane was 5.0 ± 0.4 MPa, and its elongation at break was 35.2 ± 7.2 %—slightly lower than that of NI-LPGD5. This is mainly because the average diameter of the Cur/NI-LPGD5 nanofibers is smaller than that of NI-LPGD5 [43].

After immersing in PBS (pH = 7.4) for 24 h, we measured the hygroscopic-swelling rate of the nanofiber membranes. As shown in Fig. 6B, the hygroscopic-swelling rate of the NIPU nanofiber film was 1600 %, and that of NI-LPGD5 was 2000 %, which is explained by NI-LPGD5 having a higher hydrophilicity than that of NIPU. However, Cur/NI-LPGD5 exhibited the lowest hygroscopic-swelling rate due to the addition of hydrophobic curcumin, but it also reached 1300 %.

As shown in Fig. 6C, we measured the water vapor transmittance (WVTR) of the nanofiber membranes. The WVTR of the NIPU, NI-LPGD5, and Cur/NI-LPGD5 nanofiber membranes reached 3462.5 ± 7.4 g/(m²·d), 3405.0 ± 24.1 g/(m²·d), and 3313.4 ± 9.3 g/(m²·d), respectively.

Finally, we peeled the Cur/NI-LPGD5 nanofiber film off and placed it on the wrist of the experimenter, as shown in Fig. 6D and Video 1. The nanofiber membrane exhibited suitable attachment with the movement of the human wrist joint, indicating its potential application in joint injuries. At the same time, the Cur/NI-LPGD5 nanofiber membrane maintained its intact structure without tears even after 6 h of application on the human wrist.

3.6. Antimicrobial properties of nanofibrous membranes

In this study, we investigated the antimicrobial activity of three different types of nanofiber membranes, namely NIPU, NI-LPGD5, and Cur/NI-LPGD5, against two types of bacteria: gram-positive *S. aureus* and gram-negative *E. coli*. As shown in Fig. 7A and B, the NI-LPGD5 nanofiber films showed antibacterial activity against *S. aureus* after 3 h of contact with *S. aureus* (>75 %). The Cur/NI-LPGD5

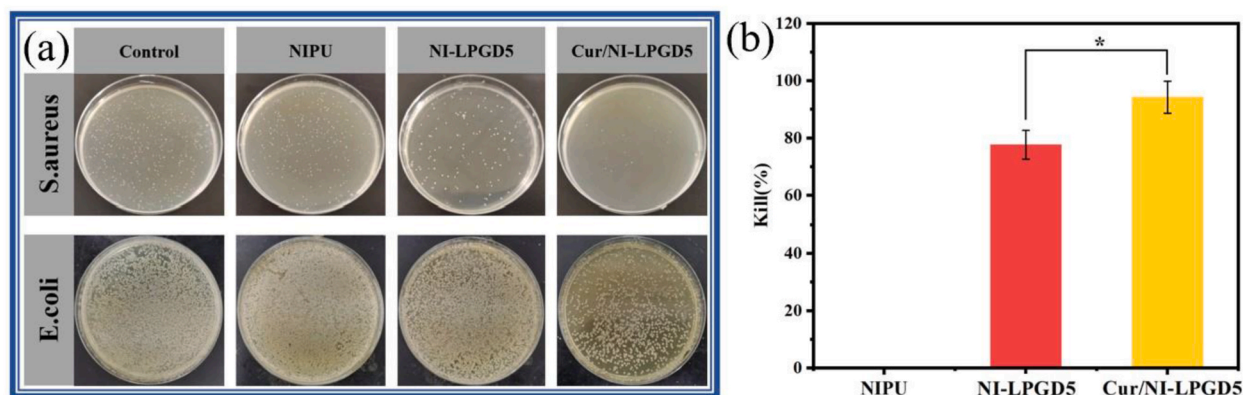


Fig. 7. Antibacterial activity of the nanofiber membranes: A) number of colonies of *S. aureus* and *E. coli* after 3 h of contact with the nanofiber membrane; B) antibacterial activity of the nanofiber membranes against *S. aureus*. * $p < 0.05$.

nanofiber films showed excellent antibacterial activity against *S. aureus* after 3 h of contact with *S. aureus* (>90 %), which was mainly attributed to the proven excellent antibacterial property of curcumin [44,45]. It was not unexpected that the NIPU nanofiber membrane did not exhibit antimicrobial activity against either bacterial species. The NI-LPGD5 and Cur/NI-LPGD5 nanofiber membranes did not show satisfactory antibacterial activity against *E. coli* compared to *S. aureus*. This phenomenon can be explained by the lipopolysaccharide structure of *E. coli*, which acts as a permeability barrier, thus increasing the resistance of the bacteria [46].

3.7. Biocompatibility of nanofibrous membranes

The biocompatibility and cytotoxicity of the NIPU and NI-LPGD5 nanofibrous membranes were evaluated by the Alamar Blue[®] assay and the LIVE/DEAD[®] Viable/Cytotoxicity assay in this study. Using the direct contact method, the same number of L929 cells were seeded directly onto the material in six-well plates. The fluorescence intensity of the cells in the control tissue culture plate (TCP) was used as a reference. As seen in Fig. 8A, the cells exhibited excellent activity on both day 1 and day 3 of incubation. On the first day, the NIPU nanofiber membrane group had 89 % cell viability, whereas the NI-LPGD5 nanofiber membrane group had 95 % cell viability ($p < 0.05$). In addition, after three days of incubation, cell viability of both membranes was higher than after one day, with 93 % for the NIPU nanofiber membrane group and 98 % for the NI-LPGD5 nanofiber membrane group ($p < 0.01$), owing to the better surface wettability of the NI-LPGD5 nanofiber membrane [47]. In addition, as seen in Fig. 8B, the NIPU and NI-LPGD5 nanofiber membranes exhibited significant cell proliferation and growth trends within three days. Moreover, it was observed that the number of cells in the NI-LPGD5 nanofiber membrane group was slightly higher than that in the NIPU nanofiber membrane group. This trend was confirmed by the LIVE/DEAD staining plot shown in Fig. 8C, where no red fluorescence emitted by dead cells was observed on either the NIPU or NI-LPGD5 nanofiber membranes.

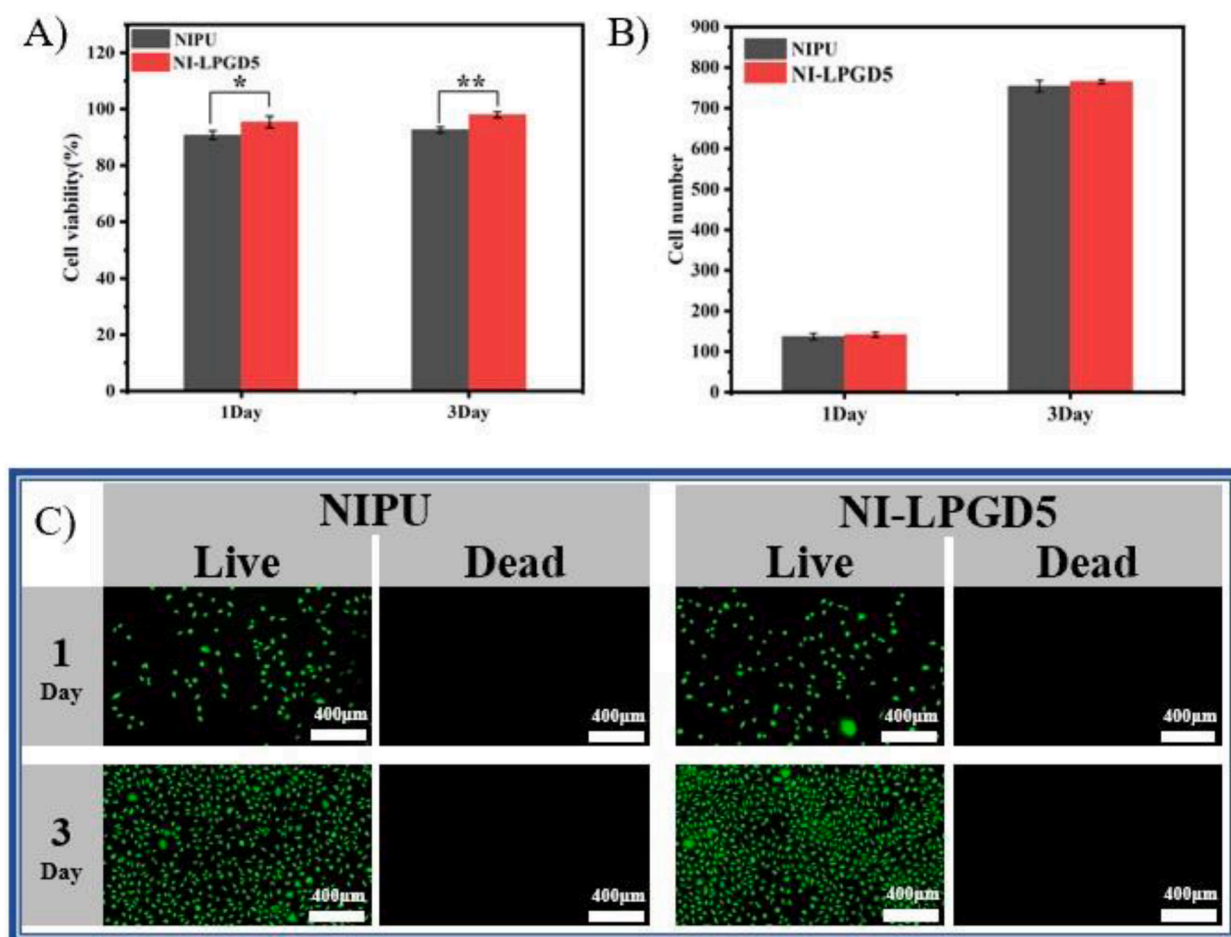


Fig. 8. Biocompatibility of the nanofiber membranes: A) biocompatibility of the nanofiber membrane; B) number of L929 cells on the nanofiber membranes after 1 and 3 days of incubation; C) fluorescence plot of LIVE/DEAD cell staining of nanofiber membranes. $*p < 0.05$; $**p < 0.01$.

3.8. *In vivo* hemostatic property of nanofibrous membranes

The hemorrhaging-liver mouse model was used to evaluate the hemostatic property of the NI-LPGD5 nanofiber membrane. A bleeding model without the nanofiber membrane was used as the control group. As shown in Fig. 9, the hemostasis effect of the nanofiber membrane group was excellent; the blood marks on the gauze were very light, and the range was small. The control group had large blood spots on the gauze, and the color was much darker. The blood loss of the control group totaled 814 ± 205 mg, and that of the nanofiber membrane group was significantly lower at 125 ± 37 mg ($p < 0.01$).

3.9. Wound healing effect of nanofiber membrane in full-thickness skin defect model

The full-thickness skin defect model experimental results of nanofiber membranes are shown Fig. 10A and B, and Fig. 10C. The wound healing rate of all the 60 mice was presented in the form of heat map, as shown in Fig. 10B. On day 5, the wound contraction rate of the experimental group was lower than that of the control group. This is due to adhesion between exposed wound tissues, which causes significant shrinkage of the wound surface; however, it also greatly increases the risk of wound infection in the control group without dressing coverage [48,49]. This effect was reflected in chronic wounds on days 10 and 15 in the control group, with the appearance of fresh, unhealed wounds or poor wound contraction. However, nanofibrous membrane can prevent tissue adhesion [50]. On day 10, all the experimental groups showed a better wound contraction rate than the control group, and the Cur/NI-LPGD5 group showed the best performance. This is because the natural structure of the nanofiber membrane and curcumin can accelerate the processes of anti-inflammation, proliferation, and remodeling [51,52]. Moreover, the median number of wound contraction rate of the NI-LPGD5 group was higher than that of the NIPU group on days 5 and 10, and the range of wound contraction rate was more concentrated than that of the NIPU group, possibly because of the antibacterial property and higher biocompatibility of the former. On day 15, regarding the number of the experimental mice with completely healed skin, namely the number of the control, NIPU, NI-LPGD5, and Cur/NI-LPGD5 groups was 4, 4, 2, 3, respectively. The experimental group did not exhibit a higher complete healing rate.

3.10. Wound granulation tissue thickness evaluation

During skin healing, the thickness of granulation tissue is considered an important evaluation index. As shown in Fig. 11A and B, the granulation tissue thickness in the NIPU, NI-LPGD5, and Cur/NI-LPGD5 groups was much larger than that in the control group after 15 days of use. The granulation tissue of the NIPU group was >650 μm thicker than that of the control group ($p < 0.01$), that of the NI-LPGD5 group was >700 μm thicker ($p < 0.01$), and that of the Cur/NI-LPGD5 group was >500 μm thicker ($p < 0.05$). These results indicated that the nanofiber membrane groups promoted granulation tissue formation better than the control group. The granulation tissue of the NI-LPGD5 group was more than that of the NIPU group. The thickness of granulation tissue in the experimental group treated with Cur/NI-LPGD5 was the thinnest, indicating adequate acceleration of the skin remodeling process as the tissue gradually differentiated into normal skin during healing [53].

3.11. Histological evaluation of wound regeneration

When skin damage occurs, timely hemostasis can help the wound to enter the healing stages of anti-inflammation, proliferation, and remodeling. The three phases are continuous and overlapping with each other [54]. In this study, we observed the histomorphological changes of the mice wounds by H&E staining. After examining the tissue sections of wound regeneration, wound

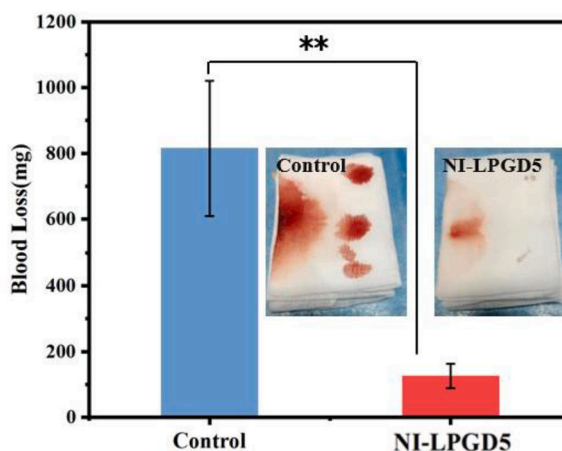


Fig. 9. *In vivo* hemostatic property of NI-LPGD5 nanofibrous membranes. $**p < 0.01$.

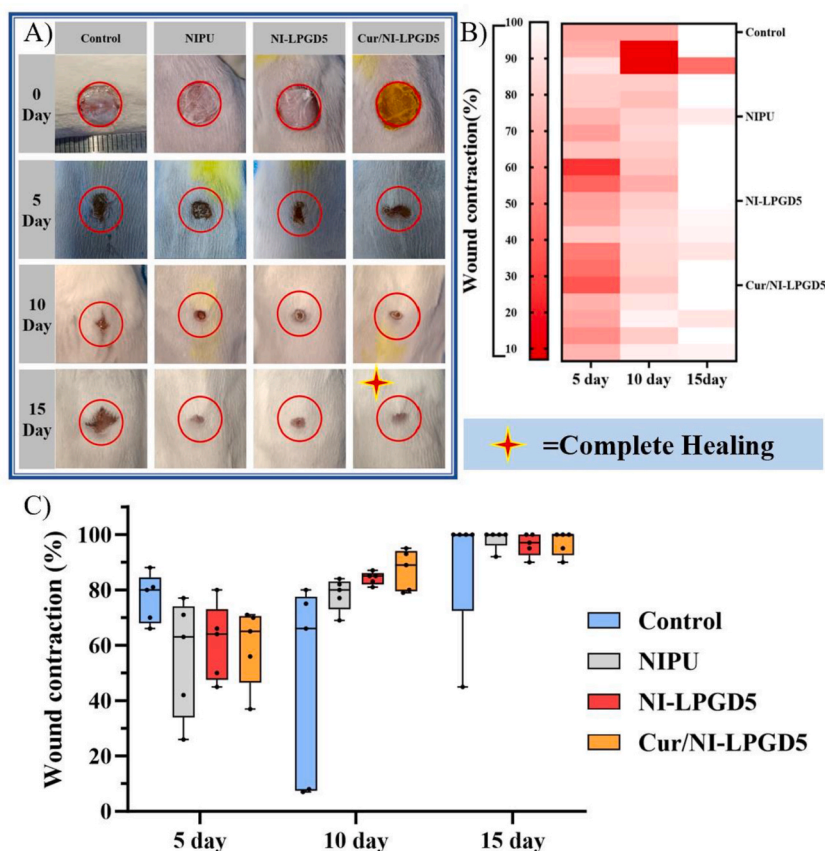


Fig. 10. Wound healing analysis of nanofibrous membranes: A) Wound healing diagram at 0, 5, 10, and 15 days; B) Heat map of wound healing rate of all the 60 mice; C) wound contraction of nanofiber membrane.

healing was evaluated by scoring epidermal injury, subcutaneous inflammation, edema and hemorrhage, growth of granulation tissue and collagen fibers, and regeneration of the skin's accessory structures. The scoring details are shown in Table 1 of the SI. The results of scoring are shown in Table 3 below. The H&E-stained sections of the wound are shown in Fig. 12. On day 5 of healing, many fibroblasts migrated to the epidermis, and the subcutaneous inflammation was maintained at a low level in the control and experimental groups. In addition, the experimental group did not exhibit excessive inflammation or skin lesions through direct contact with the dressing. Thus, all these dressings have excellent biocompatibility. We observed less subcutaneous edema and hemorrhage in the experimental group compared to the control group owing to the nanofiber membrane effectively blocking bacterial invasion and curcumin having good anti-inflammatory activity [54,55]. On day 10 of healing, wounds in the control group healed poorly and tended to become chronic, with a large number of abscesses on the surface and significant infiltration of inflammatory cells. Compared with the control group, the experimental group did not develop chronic wounds, proving that the nanofiber membrane can effectively prevent wounds becoming chronic. The wound surface was entirely covered by both epithelial and connective tissue in the experimental group. At the same time, the appearance of hair follicle structure in the NI-LPGD5 and Cur/NI-LPGD5 groups indicated that these two groups of nanofibrous membranes promoted skin tissue recovery. One possible explanation is that NI-LPGD5 can better promote the activity of fibroblasts and keratinocytes, and the ECM-like structure of the nanofibrous membrane and curcumin can enhance the epithelialization of skin tissue [14,56,57]. On day 15 of healing, complete epithelial and dermal structures were formed in the control, NIPU, NI-LPGD5, and Cur/NI-LPGD5 groups, and complete wound healing was observed in some individuals. However, individuals in the control group still developed chronic wounds, whereas no chronic wounds were found in the three nanofiber membrane groups. Once again, nanofiber membranes effectively inhibited acute wounds becoming chronic. The control and experimental groups showed some noticeable hair follicle structures. However, the NIPU group had fewer hair follicles relatively, and the arrangement of the various tissues was not as regular as that in the NI-LPGD5 and Cur/NI-LPGD5 groups. In contrast, the NI-LPGD5 and Cur/NI-LPGD5 nanofibrous membrane exhibited better performance, which resulted in a faster wound re-epithelialization process, a more regular and neatly arranged skin tissue structure, a higher number of hair follicles, and a better healing effect. In addition, in the deep skin of the Cur/NI-LPGD5 nanofiber membrane group, numerous adipose structures were observed, indicating superior healing.

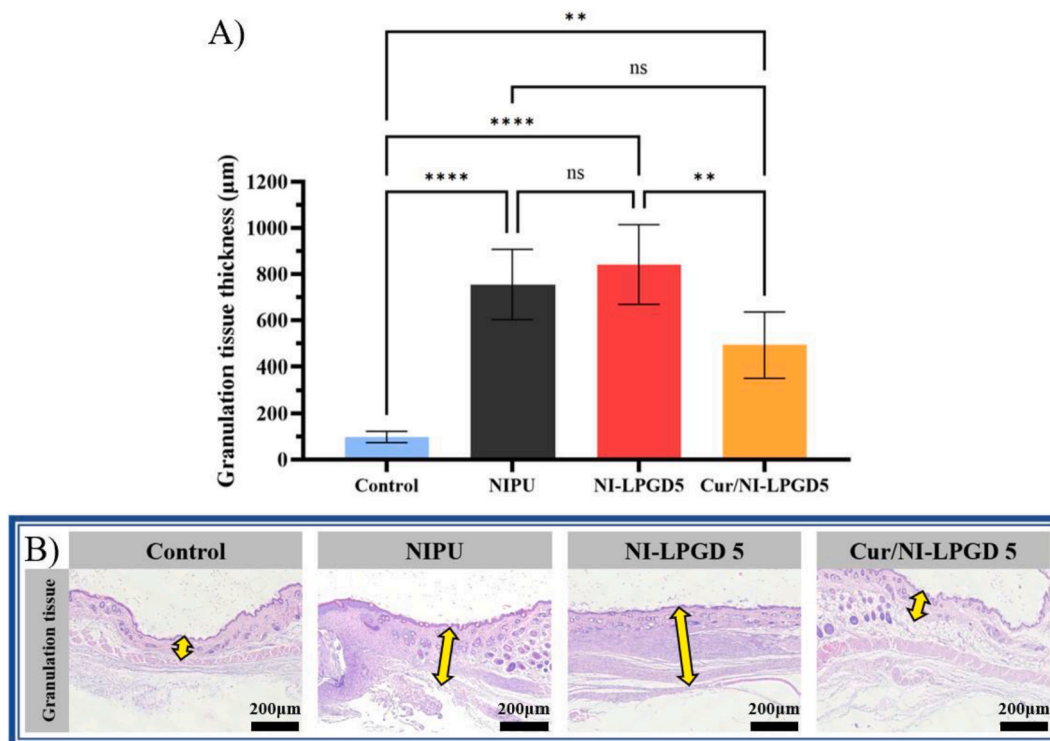


Fig. 11. Wound granulation tissue thickness: A) granulation tissue thickness of wounds at day 15; B) H&E staining of granulation tissue thickness at day 15. * $p < 0.05$; ** $p < 0.01$; **** $p < 0.0001$.

3.12. Biomarker analysis of wound regeneration

TGF- β 1 is a pleiotropic cytokine with a demonstrated pro-fibrotic and pro-inflammatory capacity. TGF- β 1 acts by modulating cellular proliferation and differentiation and induces the generation of extracellular-matrix components and transcription of pro-collagen I and II, which in turn facilitate wound healing and tissue repair [58–60]. Fig. 13A shows the expression level of TGF- β 1 during the wound healing process of mice in the NIPU, NI-LPGD5 and Cur/Ni-LPGD5 groups on days 5, 10 and 15. On day 5, the TGF- β 1 expression level of Cur/Ni-LPGD5 in the experimental groups was the highest ($p < 0.001$), indicating that curcumin significantly promoted TGF- β 1 release. The expression of TGF- β 1 in the NIPU and NI-LPGD5 groups was significantly lower than that in the control group (NI-LPGD5, $p < 0.001$). This is because the NIPU and NI-LPGD5 nanofiber membranes groups block bacterial invasion, so the body does not need to secrete much TGF- β 1 to recruit inflammatory cells. On day 10, the expression levels of TGF- β 1 in the NIPU and NI-LPGD5 groups were significantly higher than in the control group ($p < 0.01$). On day 15, the expression levels of TGF- β 1 in the experimental groups were not statistically different from that of the control group. However, the expression level of TGF- β 1 in the Cur/Ni-LPGD5 group was considerably higher than that of the other experimental groups ($p < 0.01$) mainly because myofibroblasts were formed during the remodeling phase of wound healing, pulling the wound to shut. The mechanical force generated by myofibroblasts pulling the wound activated the expression of TGF- β 1 [61,62]. Fig. 11B shows that the Cur/Ni-LPGD5 nanofibrous membrane promoted the formation of muscle fibers during wound remodeling.

VEGF-A, an important member of the VEGF family, acts as the primary regulator of angiogenesis and also plays an essential proangiogenic factor that stimulates endothelial cells to differentiate, proliferate, migrate, and survive, leading new blood vessel formation [63–65]. Fig. 13B shows the expression levels of VEGF-A during the wound healing process of mice in the NIPU, NI-LPGD5 and Cur/Ni-LPGD5 groups on days 5, 10 and 15. On day 5, the expression levels of VEGF-A in the experimental groups were higher than that in the control group, and the expression level of VEGF-A in the NI-LPGD5 group was the highest ($p < 0.01$). The hydrophilicity and ECM-like structure of the nanofiber membranes could adsorb more fibroblasts and platelets, and secrete more VEGF-A than the control group [29,66]. In contrast to the NI-LPGD5 group, the expression level of VEGF-A decreased in the Cur/Ni-LPGD5 group. This is mainly because wounds are rich in oxidants; studies have shown that these oxidants do not necessarily contribute to injury but have a role in promoting angiogenesis [63]. As a phenolic antioxidant, curcumin can effectively inhibit the expression of the VEGF-A gene [67,68]. On day 10, the expression levels of VEGF-A in the experimental groups were higher than that in the control group, and the NI-LPGD5 and Cur/Ni-LPGD5 groups showed statistically significant differences compared to the control group ($p < 0.05$). This was associated with thicker granulation tissue in the experimental groups. On day 15, the expression of VEGF-A was lower in the NIPU and NI-LPGD5 groups than in the control group, which may be due to better vascular healing in the former two groups, reducing the need for excess VEGF-A. However, the expression level of VEGF-A in the Cur/Ni-LPGD5 group was higher than that of the other two groups of

Table 3

Histopathological observation after the application of different nanofiber membranes on the full-thickness skin defect model in mice.

Histopathological observation	5 Day				10 Day				15 Day			
	Control	NIPU	NI-LPGD5	Cur/NI-LPGD5	Control	NIPU	NI-LPGD5	Cur/NI-LPGD5	Control	NIPU	NI-LPGD5	Cur/NI-LPGD5
Epidermal damage	+++	+++	+++	+++	+	+	+	+	-	+	+	-
Subcutaneous inflammation	++	++	++	++	++	++	++	++	-	-	+	-
Edema and hemorrhage	++	+	+	+	+	+	+	-	-	-	+	-
Granulation tissue and collagen fibers	++	++	++	++	++	+	++	+	+++	+	+	+
Regeneration of accessory structures	+++	+++	+++	+++	+++	++	+++	++	+	++	+	-

Scored as Severe (+++); Moderate (++); Mild (+); and Not Present (-).

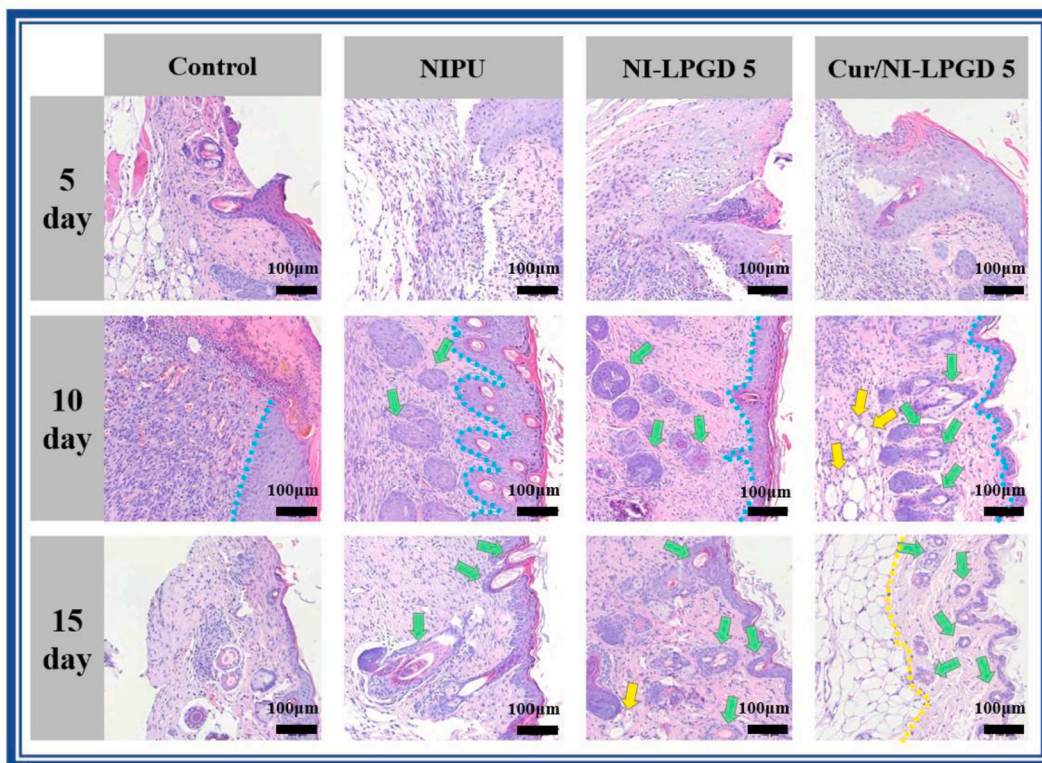


Fig. 12. Histomorphological evaluation of wound regeneration with nanofibrous membrane (hair follicles: green arrows, adipose cell: yellow arrows, boundary of epidermum and dermum: blue lines, boundary of adipocyte layer and dermum: yellow line).

nanofibrous membranes.

4. Discussion

Compared to other types of wound dressings, nanofiber membranes have significant potential demonstrated in preventing the formation of chronic wounds due to their unique micro/nano pores. Additionally, the selection of an appropriate dressing basal material is crucial in order to minimize the risk of excessive immune rejection and reduce the frequency of dressing changes significantly. In our study, we prepared a promising bioactive membrane by electrospinning using LPGD (with exceptional biocompatibility and biodegradability) and NIPU (the synthetic path is green and nontoxic) as base materials for wound dressings and applied it to wound management, especially in preventing chronic wound formation and reducing the frequency of dressing changes.

In this study, LPGD with a double-terminal hydroxyl group structure was synthesized and copolymerized with NIPU to prepare NI-LPGD. The successful synthesis of LPGD and NI-LPGD was demonstrated through the utilization of FT-IR, acid value, ^1H NMR, and XPS techniques.

As medical dressings can quickly stop bleeding after trauma, protect the wound from bacterial invasion, and promote wound healing, they can be regarded as the “temporary skin” of the human body before the wound is healed. Therefore, when designing wound dressings, it is necessary to consider whether the substrate’s physical properties (e.g., mechanical and hydrophilic properties) are satisfied. In mechanical property testing, the NI-LPGD5 exhibited the highest elongation at break. However, the tensile strength of the NI-LPGD5 was lower than that of NIPU. This is because the oxygen atom on the ester group of LPGD can easily form an intermolecular hydrogen bond with the hydrogen atom on the carbamate group of NIPU. The formation of the carbamate bond crystal structure was hindered to some extent, resulting in the crystallinity of NI-LPGD5 being lower than that of NIPU. The decrease in crystallinity increased the toughness of the material to some extent [69]. Although the tensile strength of NI-LPGD5 is lower than that of NIPU, it still reaches 11 MPa, which is a suitable basal material of wound dressings.

Studies have shown that hydrophilic materials can improve cell adhesion, reduce rejection, and establish direct contact with the wound area [29]. After conducting hydrophilicity tests, we found that the hydrophilicity of the NI-LPGD can be significantly enhanced through the incorporation of LPGD. But the hydrophilicity of NI-LPGD15 and NI-LPGD20 decreased as the content of LPGD increased. This is because, during the synthesis of NI-LPGD, an amidation reaction occurred between HFIP and SAC, forming bis(1,1,1,3,3,3-hexafluoropropane-2-yl) decanedioate (BHFD). Consequently, a trifluoromethyl residue was introduced into the copolyester, which led to a reduction in the material’s hydrophilicity [70]. In addition, the presence of BHFD as an impurity in NI-LPGD further reduced the material’s elongation at break [71]. As a consequence, the mechanical properties of NI-LPGD15 and NI-LPGD20 were

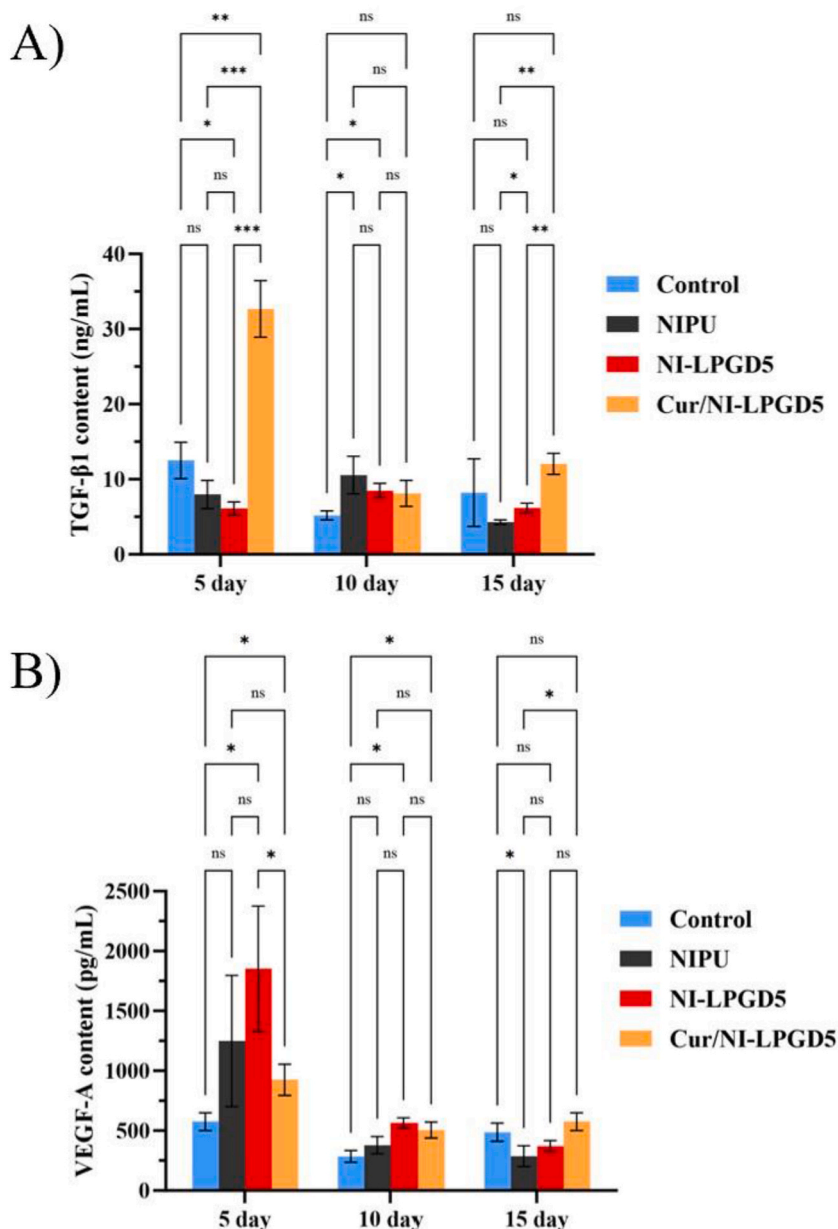


Fig. 13. Degree of relevant gene expression: A) TGF-β1; and B) VEGF-A. * $p < 0.05$, ** $p < 0.01$, *** $p < 0.001$.

significantly diminished in comparison to those of NI-LPGD5. In conclusion, we selected NI-LPGD5 as the material for the preparation of nanofiber membranes in this study due to its mechanical properties, hydrophilicity, and minimal BHFH residue.

The addition of bioactive substances to achieve various biomedical applications is also a common strategy when designing wound dressings [72]. In this study, curcumin, a substance widely shown to regulate the regeneration of skin tissue and function during wound healing [73], was added to NI-LPGD5 as a drug load to produce a Cur/Ni-LPGD5 nanofiber membrane.

The SEM of nanofiber membranes showed that adding LPGD did not affect the average diameter of the nanofibers but did increase their uniformity. Meanwhile, the average diameter of the Cur/Ni-LPGD5 nanofibers was smaller than that of the NIPU and NI-LPGD5 nanofibers, mainly because curcumin is an antioxidant substance that carries a positive charge. This positive charge increases the charge density on the Taylor cone, which causes the spinning solution jet to be subjected to more tensile force in the electric field. As a result, thinner and more uniform nanofibers are produced [67,74]. Porosity calculations showed that the porosity of these nanofibrous membranes was >60%. The interconnected pores increase the efficiency of gas exchange and promote the transport of nutrients and metabolites, which can be used as an excellent skin matrix to create favorable conditions for wound healing [75–77].

As a replacement for skin after damage, wound dressings need to have physical characteristics similar to those of normal human

skin [22]. Therefore, it is imperative to design wound dressings with good physical properties, including mechanical properties, hygroscopic-swelling rate, oxygen transmittance, and water vapor transmittance. In mechanical property testing, the tensile strength and elongation at break of the NI-LPGD5 nanofiber membrane were better than that of the NIPU nanofiber membrane. This difference is explained by LPGD, as a polymer with a simple linear fat structure, having a denser hydrogen bond acceptor than NIPU, which can form denser hydrogen bonds with NIPU molecular chains, thereby improving the mechanical properties of the nanofiber membrane. The mechanical properties of Cur/NI-LPGD5 nanofiber membrane were slightly lower than those of NI-LPGD5. Although these nanofibrous membranes have different mechanical properties, they all closely resemble normal human skin [78,79]. A reasonable hygroscopic-swelling rate can achieve rapid coagulation and absorption of wound exudate, and promote cell migration and proliferation [80]. The results of hygroscopic-swelling experiments showed that our preparation of nanofiber membrane had the very high hygroscopic-swelling rate. In addition to the ability of the nanofiber membrane to quickly absorb wound exudate, it is also worth considering whether it can discharge excess water timely to prevent the wound surface from becoming too wet [75]. The results of WVTR test indicated that these nanofiber membranes can effectively remove water from wounds, thereby preventing the creation of a humid environment that can facilitate the growth of harmful bacteria. In addition, the high WVTR also indicated that these nanofibrous membranes have high oxygen permeability and can prevent the propagation of anaerobic bacteria in the wound. Taken together, these excellent physical properties are sufficient to indicate that the nanofibrous membranes prepared in this study are an ideal candidate for wound dressing.

When developing materials for applications in related fields such as biomedicine, priority should be given to their biocompatibility and toxicity to biological somatic cells [81,82]. The results of biocompatibility test indicated that the NIPU and NI-LPGD5 nanofiber membranes had excellent biocompatibility and very low cytotoxicity. The NI-LPGD5 membrane is better, making it a promising candidate material for wound dressing.

Although the microscale-pores of the nanofiber membranes can prevent the invasion of foreign microorganisms, the bactericidal ability of the base materials is still attractive. The results of bacterial experiments demonstrated that the NI-LPGD5 nanofiber membrane unexpectedly exhibited a certain level of antibacterial activity against *S. aureus*. This is because the NI-LPGD5 nanofiber membrane contains a certain amount of fluorine. Fluorine, a strong electron-withdrawing element, can make a potential difference with the negatively charged cell membrane, thus affecting the integrity of the cell structure, leading to cell death [83,84]. Our XPS experiments detected the presence of fluorine element in NI-LPGD5. However, the presence of residual fluorine should be avoided during the preparation of medical materials. Therefore, in future research, it is necessary to identify a solvent with strong polarity, volatility, and absence of hydroxyl groups for the NI-LPGD synthesis process.

When applied to a wound, electrospun nanofiber membranes, as having numerous pore structures, can quickly absorb blood and promote platelet aggregation for rapid hemostasis [15]. At the same time, studies have demonstrated that the surface polarity of polyurethane materials can cause blood coagulation by promoting the deposition of fibrin and platelets [85,86]. The current study also shows that the structure of polyurethane's microphase separation has an adsorption effect on protein, which increases as the degree of microphase separation decreases [87]. This can effectively promote fibrin aggregation at the wound site, thereby promoting wound healing. In our study, the 70 % hard segment content of NIPU and the low polarity of PEG resulted in a very low degree of microphase separation of NIPU, thus achieving a better adsorption effect toward fibrin. The NI-LPGD5 nanofibrous membrane was chosen for *in vivo* hemostasis studies because of their excellent hydrophilicity, high hygroscopic swelling rate, low biotoxicity, and good flexibility. The results of *in vivo* hemostatic experiments showed that the NI-LPGD5 nanofibrous membrane had excellent *in vivo* hemostatic property. The adsorption of platelets by polyurethane, hydrophilic polyglycolic acid, and the natural pores of the nanofibrous membrane may play a synergistic role in hemostasis *in vivo* [15,88]. Therefore, these nanofiber membranes possess excellent mechanical properties, high hygroscopic-swelling rate, biocompatibility, and good hemostatic properties, making them effective hemostatic barriers with good prospects in replacing gauze for hemostasis in surgery.

To investigate the healing effect of the nanofiber membranes, we tested them on a full-thickness skin defect model, and the histomorphology of the wound tissue was examined. We observed that the pro-healing effect of the NI-LPGD5 nanofiber membrane was superior to that of NIPU, primarily due to the enhanced biocompatibility conferred by LPGD. Compared with other traditional dressings, the exceptional hydrophilicity of NI-LPGD5 nanofiber membrane dressings facilitates increased cell migration and proliferation on the dressings. Simultaneously, its excellent biocompatibility reduces immune system stimulation, minimizes white blood cell infiltration, and decreases dressing replacement frequency. Furthermore, the nanofibrous membrane's barrier property effectively safeguards against microbial colonization and prevent wound from progressing into a chronic state. We also found that Cur/NI-LPGD5 nanofiber membranes exhibited the best effect among these nanofiber membranes in terms of wound healing due to the addition of curcumin. In addition to curcumin, the incorporation of multiple drugs into the NI-LPGD5 nanofiber membranes synthesized in this study can be utilized for targeted treatment of specific diseases. Simultaneously, the exceptional biocompatibility of the nanofiber membrane is advantageous for extending its lifespan and facilitating enhanced drug release. Moreover, this remarkable biocompatibility also enables the utilization of nanofibrous membranes as an *in vivo* drug delivery system without concerns regarding immune rejection.

The rationale of biomarkers is to provide information about biological processes by measuring the presence or activity levels of specific molecules and substances in an organism [89]. At the same time, biomarkers play a key role in objectively assessing wound status, providing quantitative indicators for the degree of wound healing, inflammation, infection and tissue regeneration. In our study, we chosen TGF- β 1 and VEGF-A as biomarkers. After evaluation, it was found that the nanofiber membrane groups had higher biomarker contents than the control group. They accelerated the wound-healing process by increasing the expression of TGF- β 1 and VEGF-A. On day 15, the Cur/NI-LPGD5 group had the best performance among the different groups. However, we also observed a wide distribution of data in some groups, potentially attributable to insufficient control over objective factors in the process of animal

experiments, such as temperature, humidity, illumination time and living space for mice.

5. Conclusions

We have prepared wound dressings with nanofiber membranes using NIPU and LPGD as substrates. The dressings could rapidly stop bleeding, effectively prevent chronic wound formation without replacement, and demonstrated effective wound protection and healing promotion effects in the full-thickness skin defect mouse model. The process of making nanofiber films involved several steps. First, LPGD was synthesized by using GA and NPG. Then, NI-LPGD5 (5 wt% LPGD) was co-synthesized with PEG-based NIPU. Finally, NIPU, NI-LPGD5, and Cur/NI-LPGD5 nanofibrous membranes were produced using the electrospinning method. The Cur/NI-LPGD5 membrane was loaded with curcumin. These nanofibrous membranes have consistent porosity, similar mechanical properties to human skin, and excellent hygroscopic-swelling rate and water vapor transmittance. Moreover, NI-LPGD5 exhibited better hydrophilicity and biocompatibility than NIPU. Antibacterial experiments showed that NI-LPGD5 and Cur/NI-LPGD5 also had excellent antibacterial activity. These nanofibrous membranes not only effectively stopped bleeding but also blocked the invasion of harmful bacteria. This effect is beneficial in preventing wounds from turning into chronic wounds, as demonstrated in both the liver hemorrhage mouse model and the full-thickness skin defect model. Additionally, the nanofibrous membranes upregulated the expression of TGF- β 1 and VEGF-A, which promoted the formation of ECM and new blood vessels, ultimately helping with wound healing. In particular, the Cur/NI-LPGD5 nanofibrous membrane showed the best wound healing effect. Based on our results, it can be concluded that the Cur/NI-LPGD5 nanofibrous membrane possesses excellent mechanical properties, water vapor transmittance, antibacterial properties, biocompatibility, and hemostasis ability; furthermore, it can effectively prevent chronic wound development and can serve as a wound dressing without requiring frequent replacement. This work provides a reference for the further application of NIPU and LPGD in the medical field.

6. Limitations of the study

Future research in this study may focus on *in vivo* biotherapeutic protocols, including the selection of drug species, determining the optimal duration of release, and exploring effective methods for peeling the nanofibrous membranes off. In our study, *S. aureus* and *E. coli* were utilized for antibacterial experiments. However, future investigations will specifically target *MDR Pseudomonas* or *MRSA* as they are the primary pathogens responsible for wound infections. Additionally, considering the various objective factors that can influence experimental data during animal studies, it is essential to increase the number of experimental subjects appropriately in future research.

Statement of ethics

All animal experiments were approved by the Animal Ethics Committee of Chengdu Sunway Experimental Animal Co., LTD. Number: DWLL-SWLAB-2023-10-24-001.

Data availability statement

Data will be made available on request.

CRediT authorship contribution statement

Fan Ge: Writing – original draft, Validation, Project administration, Investigation, Formal analysis, Data curation, Conceptualization. **Tong Wan:** Writing – review & editing, Project administration, Funding acquisition, Conceptualization. **Linling Kong:** Methodology, Data curation. **Bowen Xu:** Methodology, Data curation. **Mengxue Sun:** Software, Methodology. **Biao Wang:** Resources, Project administration. **Shubo Liang:** Supervision, Methodology. **Hao Wang:** Resources. **Xia Zhao:** Methodology, Data curation.

Declaration of competing interest

The authors declare that they have no known competing financial interests or personal relationships that could have appeared to influence the work reported in this paper.

Acknowledgements

This work was supported by the College of Chemical Engineering and Material Science of Tianjin University of Science and Technology. We also thank Prof. Hao Wang and Xia Zhao at the College of Food Science and Engineering of Tianjin University of Science and Technology for their help with the antibacterial experiments.

Appendix A. Supplementary data

Supplementary data to this article can be found online at <https://doi.org/10.1016/j.heliyon.2024.e33693>.

References

- [1] Y. Liang, Y. Liang, H. Zhang, B. Guo, Antibacterial biomaterials for skin wound dressing, *Asian J. Pharm. Sci.* 17 (2022) 353–384, <https://doi.org/10.1016/j.ajps.2022.01.001>.
- [2] Z. Fan, B. Liu, J. Wang, S. Zhang, Q. Lin, P. Gong, L. Ma, S. Yang, A novel wound dressing based on Ag/graphene polymer hydrogel: effectively kill bacteria and accelerate wound healing, *Adv. Funct. Mater.* 24 (2014) 3933–3943, <https://doi.org/10.1002/adfm.201304202>.
- [3] R. Dong, Y. Jia, C. Qin, L. Zhan, X. Yan, L. Cui, Y. Zhou, X. Jiang, Y. Long, In situ deposition of a personalized nanofibrous dressing via a handy electrospinning device for skin wound care, *Nanoscale* 8 (2016) 3482–3488, <https://doi.org/10.1039/C5NR08367B>.
- [4] Z. Di, Z. Shi, M.W. Ullah, S. Li, G. Yang, A transparent wound dressing based on bacterial cellulose whisker and poly(2-hydroxyethyl methacrylate), *Int. J. Biol. Macromol.* 105 (2017) 638–644, <https://doi.org/10.1016/j.ijbiomac.2017.07.075>.
- [5] M. Asama, A. Hall, Y. Qi, B. Moreau, H. Walthier, M. Schaschvary, B. Bristow, Q. Wang, Alternative foaming agents for topical treatment of ulcerative colitis, *J. Biomed. Mater. Res.* 106 (2018) 1448–1456, <https://doi.org/10.1002/jbm.a.36324>.
- [6] K. Chen, H. Hu, Y. Zeng, H. Pan, S. Wang, Y. Zhang, L. Shi, G. Tan, W. Pan, H. Liu, Recent advances in electrospun nanofibers for wound dressing, *Eur. Polym. J.* 178 (2022) 111490, <https://doi.org/10.1016/j.eurpolymj.2022.111490>.
- [7] C.D. Weller, V. Team, G. Sussman, First-line interactive wound dressing update: a comprehensive review of the evidence, *Front. Pharmacol.* 11 (2020) 495485, <https://doi.org/10.3389/fphar.2020.00155>.
- [8] X. Zhao, H. Wu, B. Guo, R. Dong, Y. Qiu, P.X. Ma, Antibacterial anti-oxidant electroactive injectable hydrogel as self-healing wound dressing with hemostasis and adhesiveness for cutaneous wound healing, *Biomaterials* 122 (2017) 34–47, <https://doi.org/10.1016/j.biomaterials.2017.01.011>.
- [9] S. Li, L. Wang, W. Zheng, G. Yang, X. Jiang, Rapid fabrication of self-healing, conductive, and injectable gel as dressings for healing wounds in stretchable parts of the body, *Adv. Funct. Mater.* 30 (2020) 2002370, <https://doi.org/10.1002/adfm.202002370>.
- [10] S. Sabra, D.M. Ragab, M.M. Agwa, S. Rohani, Recent advances in electrospun nanofibers for some biomedical applications, *Eur. J. Pharmaceut. Sci.* 144 (2020) 105224, <https://doi.org/10.1016/j.ejps.2020.105224>.
- [11] M.L. Patton, R.F. Mullins, D. Smith, R. Korentager, An open, prospective, Randomized Pilot investigation evaluating Pain with the Use of a Soft Silicone wound contact layer vs bridal veil and staples on split thickness skin grafts as a primary dressing, *J. Burn Care Res.* 34 (2013) 674–681, <https://doi.org/10.1097/BCR.0b013e3182853c6d>.
- [12] E.A. Kamoun, E.R.S. Kenawy, X. Chen, A review on polymeric hydrogel membranes for wound dressing applications: PVA-based hydrogel dressings, *J. Adv. Res.* 8 (2017) 217–233, <https://doi.org/10.1016/j.jare.2017.01.005>.
- [13] H.T. Bui, O.H. Chung, J. Dela Cruz, J.S. Park, Fabrication and characterization of electrospun curcumin-loaded polycaprolactone-polyethylene glycol nanofibers for enhanced wound healing, *Macromol. Res.* 22 (2014) 1288–1296, <https://doi.org/10.1007/s13233-014-2179-6>.
- [14] S.G. Priya, A. Gupta, E. Jain, J. Sarkar, A. Damania, P.R. Jagdale, B.P. Chaudhari, K.C. Gupta, A. Kumar, Bilayer cryogel wound dressing and skin regeneration grafts for the treatment of acute skin wounds, *ACS Appl. Mater. Interfaces* 8 (2016) 15145–15159, <https://doi.org/10.1021/acsami.6b04711>.
- [15] J. Chen, L. Lv, Y. Li, X. Ren, H. Luo, Y. Gao, H. Yan, Y. Li, Y. Qu, L. Yang, Preparation and evaluation of Bletilla striata polysaccharide/graphene oxide composite hemostatic sponge, *Int. J. Biol. Macromol.* 130 (2019) 827–835, <https://doi.org/10.1016/j.ijbiomac.2019.02.137>.
- [16] J. Yang, L. Xu, Electrospun nanofiber membranes with various structures for wound dressing, *Materials* 16 (2023) 6021, <https://doi.org/10.3390/ma16176021>.
- [17] F. Croisier, C. Jérôme, Chitosan-based biomaterials for tissue engineering, *Eur. Polym. J.* 49 (2013) 780–792, <https://doi.org/10.1016/j.eurpolymj.2012.12.009>.
- [18] T. Zhou, N. Wang, Y. Xue, T. Ding, X. Liu, X. Mo, J. Sun, Development of biomimetic tilapia collagen nanofibers for skin regeneration through inducing keratinocytes differentiation and collagen synthesis of dermal fibroblasts, *ACS Appl. Mater. Interfaces* 7 (2015) 3253–3262, <https://doi.org/10.1021/am507990m>.
- [19] N. Siddiqui, S. Asawa, B. Birru, R. Baadhe, S. Rao, PCL-based composite scaffold matrices for tissue engineering applications, *Mol. Biotechnol.* 60 (2018) 506–532, <https://doi.org/10.1007/s12033-018-0084-5>.
- [20] Y. Chen, J. Lin, Y. Wan, Y. Fei, H. Wang, W. Gao, Preparation and blood compatibility of electrospun PLA/curcumin composite membranes, *Fibers Polym.* 13 (2012) 1254–1258, <https://doi.org/10.1007/s12221-012-1254-x>.
- [21] G. Kasi, S. Gnanasekar, K. Zhang, E.T. Kang, L.Q. Xu, Polyurethane-based composites with promising antibacterial properties, *J. Appl. Polym. Sci.* 139 (2022) 52181, <https://doi.org/10.1002/app.52181>.
- [22] M. Morales-González, L.E. Díaz, C. Dominguez-Paz, M.F. Valero, Insights into the design of polyurethane dressings suitable for the stages of skin wound-healing: a systematic review, *Polymers* 14 (2022) 2990, <https://doi.org/10.3390/polym14152990>.
- [23] J.E. Lockey, C.A. Redlich, R. Streicher, A. Pfahles-Hutchens, P.B.J. Hakkinen, G.L. Ellison, P. Harber, M. Utell, J. Holland, A. Comai, Isocyanates and human health: multistakeholder information needs and research priorities, *J. Occup. Environ. Med.* 57 (2015) 44–51, <https://doi.org/10.1097/JOM.0000000000000278>.
- [24] W.N. Rom, S.B. Markowitz, *Environmental and Occupational Medicine*, Lippincott Williams & Wilkins, 2007.
- [25] D.C. Allport, D.S. Gilbert, S. Outterside, MDI and TDI: Safety, Health and the Environment: a Source Book and Practical Guide, John Wiley & Sons, 2003.
- [26] W.Y. Chen, H.Y. Chang, J.K. Lu, Y.C. Huang, S.G. Harroun, Y.T. Tseng, Y.J. Li, C.C. Huang, H.T. Chang, Self-assembly of antimicrobial peptides on gold nanodots: against multidrug-resistant bacteria and wound-healing application, *Adv. Funct. Mater.* 25 (2015) 7189–7199, <https://doi.org/10.1002/adfm.201503248>.
- [27] J. Lin, C. Li, Y. Zhao, J. Hu, L. Zhang, Co-electrospun nanofibrous membranes of collagen and zein for wound healing, *ACS Appl. Mater. Interfaces* 4 (2012) 1050–1057, <https://doi.org/10.1021/am201669z>.
- [28] X. Liu, L. You, S. Tarafder, L. Zou, Z. Fang, J. Chen, C.H. Lee, Q. Zhang, Curcumin-releasing chitosan/alginate membrane for skin regeneration, *Chem. Eng. J.* 359 (2019) 1111–1119, <https://doi.org/10.1016/j.cej.2018.11.073>.
- [29] Z. Pahlevanneshan, M. Deypour, A. Kefayat, M. Rafienia, P. Sajkiewicz, R. Esmaeely Neisiany, M.S. Enayati, Polyurethane-nanolignin composite foam coated with propolis as a platform for wound dressing: synthesis and characterization, *Polymers* 13 (2021) 3191, <https://doi.org/10.3390/polym13183191>.
- [30] B.D. Ulery, L.S. Nair, C.T. Laurencin, Biomedical applications of biodegradable polymers, *J. Polym. Sci. B Polym. Phys.* 49 (2011) 832–864, <https://doi.org/10.1002/polb.22259>.
- [31] V. Sanko, I. Sahin, U. Aydemir Sezer, S. Sezer, A versatile method for the synthesis of poly (glycolic acid): high solubility and tunable molecular weights, *Polym. J.* 51 (2019) 637–647, <https://doi.org/10.1038/s41428-019-0182-7>.
- [32] J.C. Middleton, A.J. Tipton, Synthetic biodegradable polymers as orthopedic devices, *Biomaterials* 21 (2000) 2335–2346, [https://doi.org/10.1016/S0142-9612\(00\)00101-0](https://doi.org/10.1016/S0142-9612(00)00101-0).
- [33] Y. Lu, C. Schmidt, S. Beuermann, Fast synthesis of high-molecular-weight polyglycolide using diphenyl bismuth bromide as catalyst, *Macromol. Chem. Phys.* 216 (2015) 395–399, <https://doi.org/10.1002/macp.201400474>.
- [34] C. Li, S. Li, J. Zhao, Z. Zhang, J. Zhang, W. Yang, Synthesis and characterization of aliphatic poly(amide urethane)s having different nylon 6 segments through non-isocyanate route, *J. Polym. Res.* 21 (2014) 1–10, <https://doi.org/10.1007/s10965-014-0498-0>.
- [35] N.H. Williamson, M. Nydén, M. Röding, The lognormal and gamma distribution models for estimating molecular weight distributions of polymers using PGSE NMR, *J. Magn. Reson.* 267 (2016) 54–62, <https://doi.org/10.1016/j.jmr.2016.04.007>.
- [36] M. Zahiri, M. Khanmohammadi, A. Goodarzi, S. Ababzadeh, M.S. Farahani, S. Mohandesnezhad, N. Bahrami, I. Nabipour, J. Ai, Encapsulation of curcumin loaded chitosan nanoparticle within poly (ϵ -caprolactone) and gelatin fiber mat for wound healing and layered dermal reconstitution, *Int. J. Biol. Macromol.* 153 (2020) 1241–1250, <https://doi.org/10.1016/j.ijbiomac.2019.10.255>.
- [37] J. Zhang, J. Li, X. Zeng, J. Wang, Y. Le, Double-layer hybrid nanofiber membranes by electrospinning with sustained antibacterial activity for wound healing, *J. Ind. Eng. Chem.* 127 (2023) 416–425, <https://doi.org/10.1016/j.jiec.2023.07.025>.

- [38] E. Lih, J.S. Lee, K.M. Park, K.D. Park, Rapidly curable chitosan-PEG hydrogels as tissue adhesives for hemostasis and wound healing, *Acta Biomater.* 8 (2012) 3261–3269, <https://doi.org/10.1016/j.actbio.2012.05.001>.
- [39] D. Wolosz, P.G. Parzuchowski, A. Świdrska, Synthesis and characterization of the non-isocyanate poly (carbonate-urethane) s obtained via polycondensation route, *Eur. Polym. J.* 155 (2021) 110574, <https://doi.org/10.1016/j.eurpolymj.2021.110574>.
- [40] G. Rokicki, A. Piotrowska, A new route to polyurethanes from ethylene carbonate, diamines and diols, *Polymer* 43 (2002) 2927–2935, [https://doi.org/10.1016/S0032-3861\(02\)00071-X](https://doi.org/10.1016/S0032-3861(02)00071-X).
- [41] M.T. Casas, J. Puiggali, J.M. Raquez, P. Dubois, M.E. Córdova, A.J. Müller, Single crystals morphology of biodegradable double crystalline PLLA-b-PCL diblock copolymers, *Polymer* 52 (2011) 5166–5177, <https://doi.org/10.1016/j.polymer.2011.08.057>.
- [42] P. Sudheesh Kumar, V.K. Lakshmanan, T. Anilkumar, C. Ramya, P. Reshmi, A. Unnikrishnan, S.V. Nair, R. Jayakumar, Flexible and microporous chitosan hydrogel/nano ZnO composite bandages for wound dressing: in vitro and in vivo evaluation, *ACS Appl. Mater. Interfaces* 4 (2012) 2618–2629, <https://doi.org/10.1021/am300292v>.
- [43] N. Alharbi, A. Daraei, H. Lee, M. Guthold, The effect of molecular weight and fiber diameter on the mechanical properties of single, electrospun PCL nanofibers, *Mater. Today Commun.* 35 (2023) 105773, <https://doi.org/10.1016/j.mtcomm.2023.105773>.
- [44] L. Qu, X. Li, J. Zhou, K. Cao, Q. Xie, P. Zhou, W. Qian, Y. Yang, A novel dual-functional coating based on curcumin/APEG polymer with antibacterial and antifouling properties, *Appl. Surf. Sci.* 627 (2023) 157224, <https://doi.org/10.1016/j.apsusc.2023.157224>.
- [45] V. Fakhri, A. Jafari, M.A. Shafiei, M.V. Ehteshamfar, S. Khalighiyan, H. Hosseini, V. Goodarzi, F.R. Wurm, M.M. Moghaddam, H.A. Khonakdar, Development of physical, mechanical, antibacterial and cell growth properties of poly (glycerol sebacate urethane)(PGSU) with helping of curcumin and hydroxyapatite nanoparticles, *Polym. Chem.* 12 (2021) 6263–6282, <https://doi.org/10.1039/D1PY01040A>.
- [46] A. Sirelkhatim, S. Mahmud, A. Seeni, N.H.M. Kaus, L.C. Ann, S.K.M. Bakhori, H. Hasan, D. Mohamad, Review on zinc oxide nanoparticles: antibacterial activity and toxicity mechanism, *Nano-Micro Lett.* 7 (2015) 219–242, <https://doi.org/10.1007/s40820-015-0040-x>.
- [47] M. Schroepfer, F. Junghans, D. Voigt, M. Meyer, A. Breier, G. Schulze-Tanzil, I. Prade, Gas-phase fluorination on PLA improves cell adhesion and spreading, *ACS Omega* 5 (2020) 5498–5507, <https://doi.org/10.1021/acsomega.0c00126>.
- [48] X. Zhao, J. Yang, Y. Liu, J. Gao, K. Wang, W. Liu, An injectable and antifouling self-fused supramolecular hydrogel for preventing postoperative and recurrent adhesions, *Chem. Eng. J.* 404 (2021) 127096, <https://doi.org/10.1016/j.cej.2020.127096>.
- [49] Z. Li, L. Liu, Y. Chen, Dual dynamically crosslinked thermosensitive hydrogel with self-fixing as a postoperative anti-adhesion barrier, *Acta Biomater.* 110 (2020) 119–128, <https://doi.org/10.1016/j.actbio.2020.04.034>.
- [50] Y. Zhao, J. Zhu, J. Zhang, Z. Chen, W. Li, L. Deng, K. Chen, H. Wan, J. Li, R. Li, Optimization of biodegradable PEG/PLGA nanofiber mats electrospinning process for anti-adhesion application, *J. Appl. Polym. Sci.* 135 (2018) 46282, <https://doi.org/10.1002/app.46282>.
- [51] D. Akbik, M. Ghadiri, W. Chrzanowski, R. Rohanizadeh, Curcumin as a wound healing agent, *Life Sci.* 116 (2014) 1–7, <https://doi.org/10.1016/j.lfs.2014.08.016>.
- [52] A. Ehterami, M. Salehi, S. Farzamfar, A. Vaez, H. Samadian, H. Sahraeyma, M. Mirzaii, S. Ghorbani, A. Goodarzi, In vitro and in vivo study of PCL/COLL wound dressing loaded with insulin-chitosan nanoparticles on cutaneous wound healing in rats model, *Int. J. Biol. Macromol.* 117 (2018) 601–609, <https://doi.org/10.1016/j.ijbiomac.2018.05.184>.
- [53] P. Mostafalu, G. Kiaee, G. Giatsidis, A. Khalilpour, M. Nabavinia, M.R. Dokmeci, S. Sonkusale, D.P. Orgill, A. Tamayol, A. Khademhosseini, A textile dressing for temporal and dosage controlled drug delivery, *Adv. Funct. Mater.* 27 (2017) 1702399, <https://doi.org/10.1002/adfm.201702399>.
- [54] V. Arul, R. Kartha, R. Jayakumar, A therapeutic approach for diabetic wound healing using biotinylated GHK incorporated collagen matrices, *Life Sci.* 80 (2007) 275–284, <https://doi.org/10.1016/j.lfs.2006.09.018>.
- [55] R. Chatterji, T. Bou-Akl, B. Wu, P. Dietz, W. Ren, D. Markel, Common wound irrigation solutions produce different responses in infected vs sterile host tissue: murine air pouch infection model, *Arthroplasty Today* 18 (2022) 130–137, <https://doi.org/10.1016/j.artd.2022.08.019>.
- [56] K.K. Chereddy, V.L. Payen, V. Pr at, PLGA: from a classic drug carrier to a novel therapeutic activity contributor, *J. Contr. Release* 289 (2018) 10–13, <https://doi.org/10.1016/j.jconrel.2018.09.017>.
- [57] J. Chen, R. Dong, J. Ge, B. Guo, P.X. Ma, Biocompatible, biodegradable, and electroactive polyurethane-urea elastomers with tunable hydrophilicity for skeletal muscle tissue engineering, *ACS Appl. Mater. Interfaces* 7 (2015) 28273–28285, <https://doi.org/10.1021/acsami.5b10829>.
- [58] B. Klass, K. Rolfe, A. Grobbelaar, In vitro flexor tendon cell response to TGF- 1: a gene expression study, *J. Hand Surg.* 34 (2009) 495–503, <https://doi.org/10.1016/j.jhssa.2008.10.032>.
- [59] S. Barrientos, O. Stojadinovic, M.S. Golinko, H. Brem, M. Tomic-Canic, Growth factors and cytokines in wound healing, *Wound Repair Regen.* 16 (2008) 585–601, <https://doi.org/10.1111/j.1524-475X.2008.00410.x>.
- [60] H.S. Dh, R. Sultana, A. Prabhu, S. Pavan, S. Mohanto, V. Subramaniyan, Biomedicine and pharmacotherapeutic effectiveness of combinatorial atorvastatin and quercetin on diabetic nephropathy: an in vitro study, *Biomed. Pharmacother.* 174 (2024) 116533, <https://doi.org/10.1016/j.biopha.2024.116533>.
- [61] B. Campbell, C. Agarwal, J. Wang, TGF- 1, TGF- 3, and PGE 2 regulate contraction of human patellar tendon fibroblasts, *Biomech. Model. Mechanobiol.* 2 (2004) 239–245, <https://doi.org/10.1007/s10237-004-0041-z>.
- [62] H. Li, S. Luo, H. Wang, Y. Chen, M. Ding, J. Lu, L. Jiang, K. Lyu, S. Huang, H. Shi, The mechanisms and functions of TGF- 1 in tendon healing, *Injury* (2023) 111052, <https://doi.org/10.1016/j.injury.2023.111052>.
- [63] S. Roy, S. Khanna, C.K. Sen, Redox regulation of the VEGF signaling path and tissue vascularization: hydrogen peroxide, the common link between physical exercise and cutaneous wound healing, *Free Radic. Biol. Med.* 44 (2008) 180–192, <https://doi.org/10.1016/j.freeradbiomed.2007.01.025>.
- [64] B. Gowda, S. Mohanto, A. Singh, A. Bhunia, M. Abdelgawad, S. Ghosh, M. Ansari, S. Pramanik, Nanoparticle-based therapeutic approaches for wound healing: a review of the state-of-the-art, *Mater. Today Chem.* 27 (2023) 101319, <https://doi.org/10.1016/j.mtchem.2022.101319>.
- [65] S. Nag, O. Mitra, P. Sankarganesh, A. Bhattacharjee, S. Mohanto, B.J. Gowda, S. Kar, S. Ramaiah, A. Anbarasu, M.G. Ahmed, Exploring the emerging trends in the synthesis and theranostic paradigms of cerium oxide nanoparticles (CeONPs): a comprehensive review, *Mater. Today Chem.* 35 (2024) 101894, <https://doi.org/10.1016/j.mtchem.2023.101894>.
- [66] F. Mi, Y. Wu, S. Shyu, A. Chao, J. Lai, C. Su, Asymmetric chitosan membranes prepared by dry/wet phase separation: a new type of wound dressing for controlled antibacterial release, *J. Membr. Sci.* 212 (2003) 237–254, [https://doi.org/10.1016/S0376-7388\(02\)00505-7](https://doi.org/10.1016/S0376-7388(02)00505-7).
- [67] D. Gopinath, M.R. Ahmed, K. Gomathi, K. Chitra, P. Sehgal, R. Jayakumar, Dermal wound healing processes with curcumin incorporated collagen films, *Biomaterials* 25 (2004) 1911–1917, [https://doi.org/10.1016/S0142-9612\(03\)00625-2](https://doi.org/10.1016/S0142-9612(03)00625-2).
- [68] R. Schindler, R. Mentlein, Flavonoids and vitamin E reduce the release of the angiogenic peptide vascular endothelial growth factor from human tumor cells, *J. Nutr.* 136 (2006) 1477–1482, <https://doi.org/10.1093/jn/136.6.1477>.
- [69] Y. Ju, Z. Qiao, H. Xiu, X. Liu, Q. Fu, H. Bai, Combined effects of matrix molecular weight and crystallinity on the impact toughness of PP/EPR blends: the role of chain entanglement, *Polymer* 272 (2023) 125863, <https://doi.org/10.1016/j.polymer.2023.125863>.
- [70] R. Koguchi, K. Jankova, M. Tanaka, Fluorine-containing bio-inert polymers: roles of intermediate water, *Acta Biomater.* 138 (2022) 34–56, <https://doi.org/10.1016/j.actbio.2021.10.027>.
- [71] K.M. Sankar, P.M. Singh, Effects of reducing impurity addition on corrosion and mechanical properties of structural materials in molten LiF-NaF-KF, *Corrosion Sci.* 227 (2024) 111702, <https://doi.org/10.1016/j.corsci.2023.111702>.
- [72] J. Chen, J. Ge, B. Guo, K. Gao, P.X. Ma, Nanofibrous polylactide composite scaffolds with electroactivity and sustained release capacity for tissue engineering, *J. Mater. Chem. B* 4 (2016) 2477–2485, <https://doi.org/10.1039/C5TB02703A>.
- [73] X. Li, K. Nan, L. Li, Z. Zhang, H. Chen, In vivo evaluation of curcumin nanoformulation loaded methoxy poly (ethylene glycol)-graft-chitosan composite film for wound healing application, *Carbohydr. Polym.* 88 (2012) 84–90, <https://doi.org/10.1016/j.carbpol.2011.11.068>.
- [74] L.M. Gradinaru, M. Bercea, S. Vlad, M.B. Mandru, M. Drobot, M. Aflori, R.C. Ciobanu, Preparation and characterization of electrospun magnetic poly (ether urethane) nanocomposite mats: relationships between the viscosity of the polymer solutions and the electrospinning ability, *Polymer* 256 (2022) 125186, <https://doi.org/10.1016/j.polymer.2022.125186>.

- [75] J. Xia, H. Zhang, F. Yu, Y. Pei, X. Luo Superclear, Porous cellulose membranes with chitosan-coated nanofibers for visualized cutaneous wound healing dressing, *ACS Appl. Mater. Interfaces* 12 (2020) 24370–24379, <https://doi.org/10.1021/acami.0c05604>.
- [76] F. Martínez-Gómez, J. Guerrero, B. Matsuhiro, J. Pavez, In vitro release of metformin hydrochloride from sodium alginate/polyvinyl alcohol hydrogels, *Carbohydr. Polym.* 155 (2017) 182–191, <https://doi.org/10.1016/j.carbpol.2016.08.079>.
- [77] A. Memic, T. Abdullah, H.S. Mohammed, K. Joshi Navare, T. Colombani, S.A. Bencherif, Latest progress in electrospun nanofibers for wound healing applications, *ACS Appl. Bio Mater.* 2 (2019) 952–969, <https://doi.org/10.1021/acsbm.8b00637>.
- [78] H. Adeli, M.T. Khorasani, M. Parvazinia, Wound dressing based on electrospun PVA/chitosan/starch nanofibrous mats: fabrication, antibacterial and cytocompatibility evaluation and in vitro healing assay, *Int. J. Biol. Macromol.* 122 (2019) 238–254, <https://doi.org/10.1016/j.ijbiomac.2018.10.11>.
- [79] X. Chen, Making electrodes stretchable, *Small Methods* 1 (2017) 1600029, <https://doi.org/10.1002/smt.201600029>.
- [80] D. Simões, S.P. Miguel, I.J. Correia, Biofunctionalization of electrospun poly (caprolactone) fibers with Maillard reaction products for wound dressing applications, *React. Funct. Polym.* 131 (2018) 191–202, <https://doi.org/10.1016/j.reactfunctpolym.2018.07.021>.
- [81] J. Qu, X. Zhao, Y. Liang, T. Zhang, P.X. Ma, B. Guo, Antibacterial adhesive injectable hydrogels with rapid self-healing, extensibility and compressibility as wound dressing for joints skin wound healing, *Biomaterials* 183 (2018) 185–199, <https://doi.org/10.1016/j.biomaterials.2018.08.044>.
- [82] C. Qin, Q. Xiao, H. Li, M. Fang, Y. Liu, X. Chen, Q. Li, Calorimetric studies of the action of chitosan-N-2-hydroxypropyl trimethyl ammonium chloride on the growth of microorganisms, *Int. J. Biol. Macromol.* 34 (2004) 121–126, <https://doi.org/10.1016/j.ijbiomac.2004.03.009>.
- [83] X. An, W. Li, Y. Zhang, J. Ding, S. Zhang, T. Hu, S. Li, Y. Ren, P. Liu, X. Li, Antibacterial and superhydrophobic hemostatic properties of fluorinated random copolymer composite nanocoatings, *Prog. Org. Coating* 168 (2022) 106869, <https://doi.org/10.1016/j.porgcoat.2022.106869>.
- [84] C. Lin, F. Luan, S. Su, A. Jiang, W. Tan, Z. Guo, Water-soluble fluorine-functionalized chitoooligosaccharide derivatives: synthesis, characterization and antimicrobial activity, *Carbohydr. Res.* 533 (2023) 108935, <https://doi.org/10.1016/j.carres.2023.108935>.
- [85] T. Groth, K. Klosz, E. Campbell, R. New, B. Hall, H. Goering, Protein adsorption, lymphocyte adhesion and platelet adhesion/activation on polyurethane ureas is related to hard segment content and composition, *J. Biomater. Sci. Polym. Ed.* 6 (1995) 497–510, <https://doi.org/10.1163/156856294X00464>.
- [86] G. Zhu, M. Wu, Z. Ding, T. Zou, L. Wang, Biological properties of polyurethane: issues and potential for application in vascular medicine, *Eur. Polym. J.* 201 (2023) 112536, <https://doi.org/10.1016/j.eurpolymj.2023.112536>.
- [87] S. Hsu, Z. Lin, Biocompatibility and biostability of a series of poly (carbonate) urethanes, *Colloids Surf. B Biointerfaces* 36 (2004) 1–12, <https://doi.org/10.1016/j.colsurfb.2004.04.003>.
- [88] X. Liu, Y. Niu, K.C. Chen, S. Chen, Rapid hemostatic and mild polyurethane-urea foam wound dressing for promoting wound healing, *Mater. Sci. Eng. C* 71 (2017) 289–297, <https://doi.org/10.1016/j.msec.2016.10.019>.
- [89] H. Singh, M. Singh, S. Nag, S. Mohanto, K. Jain, A. Shrivastav, A.K. Mishra, J. Pallavi, A. Bhunia, V. Subramaniyan, Isolation and characterization of secondary metabolites from *Bryophyllum pinnatum* (Lam.) Oken and assessment of wound healing efficacy using animal model, *South Afr. J. Bot.* 169 (2024) 531–542, <https://doi.org/10.1016/j.sajb.2024.05.008>.